Available online at www.sciencedirect.com
SCIENCE DIRECT®
Coordination Chemistry Reviews 238–239 (2003) 31–53
COORDINATION CHEMISTRY REVIEWS
www.elsevier.com/locate/ccr

Evolution of classical/quantum methodologies: applications to oxide surfaces and interfaces

D.E. Ellis *, O. Warschkow

Department of Physics and Astronomy, Institute of Environmental Catalysis, Northwestern University, 2145 No. Sheridan Rd., Evanston, IL 60208, USA

Received 2 July 2002; accepted 6 January 2003

Contents

* Corresponding author. Tel.: +1-708-491-3665; fax: +1-708-491-9982.
E-mail address: don-ellis@northwestern.edu (D.E. Ellis).

0010-8545/03/$ - see front matter
doi:10.1016/S0010-8545(03)00004-3

Abstract

First-principles quantum chemical approaches have evolved in the direction of greater precision for describing properties of small molecules, and with reduced precision, to the description of macromolecules and extended systems. However, traditional methodologies are inadequate to meet the increasing demands for time- and temperature-dependent analyses of molecular and particulate structure–function relations. We describe several of the extant hybrid classical/quantum schemes which have been evolving to meet the challenge of bridging size scales from 1 to 1000 Å and time scales from 1 to 10^7 fs. The current state of affairs is illustrated with examples of applications to metal oxide surfaces and interfaces, and future trends are discussed.

1. Introduction

The search for appropriate and approximate schemes for treating time- and temperature-dependent properties of materials has accelerated in recent years, propelled by experimental advances and the often-expressed hope of obtaining some day 'materials by design'. It has been recognized in such widely disparate areas of applied science as pharmacology, semiconductor electronics, magnetic data storage, and automotive design that there exist data at the distance scale of Angstrom and time scale of femtosec which are critical to desired materials performance. As control of materials properties has focused more and more upon the mesoscale of nanometers to microns, the need to couple analysis of atomic-scale processes to those at the mesoscale has become increasingly obvious.

Given the present state of first-principles theory and the performance of existing computers, direct solutions of the time-dependent Schrödinger (or better, Dirac) equation are feasible for only a small subset of systems of current interest. Beyond these limitations, we face the imperative to treat temperature-dependent properties with implications of ensemble behavior and statistical response, which do not form a part of traditional wave mechanics.

Thus, the development of hybrid classical/quantum methodologies can be seen as an obvious response to the 'push' of applied materials science. In this way, quantum theory is applied to manageable fragments of the extended system, and classical dynamics and statistical mechanics is used as a feasible framework for modeling on the larger scale. The construction and verification of adequate parameterized interatomic potentials which can reproduce experimental features and incorporate evolving theoretical data is a key mechanism linking the two modeling components. The development of feedback paths between quantum mechanical analyses and classical modeling remains an important area for ongoing development, as are efforts to construct data bases which can be used at the next levels, of semi-continuum and continuum simulations. In this article we review several of the extant methologies, endeavoring to point out their relative merits and opportunities for further extension. Principles and procedures are illustrated by considering examples from applications to metal oxide surfaces and interfaces.

2. Overview of quantum and classical simulation methodologies

2.1. Background

We can begin our discussion of simulation methodologies at first principles. The time-dependent Schrödinger (and its relativistic counterpart, Dirac) equation contains both nuclear **X** and electronic **x** degrees of freedom, so why not solve $H\psi = i\hbar\partial\psi/\partial t$ directly for their joint time dependence $\Psi(\mathbf{X}, \mathbf{x})$? Then repeat this scheme for an ensemble of states of different energy E_i and apply the well-known theorems of statistical mechanics to extract the T-dependence? Alas, as we learn in a first-year quantum mechanics course, the wavefunction is horribly complex for two or more particles and is in any case bound to be an overkill [1]. Conveniently-at least for the majority of applications discussed in this review—there exists an approximate separation of electronic and nuclear degrees of motion, dividing the problem into two that can be dealt with separately, sequentially, or in parallel. As was shown long ago by Born and Oppenheimer, the large relative mass difference between electrons and nuclei leads to a partial decoupling of their motions. To a good approximation, the electrons are dragged along by the nuclei, and the dressed nuclei (atoms in molecules) move in the field of the electronic distribution [2]. In such adiabatic scenarios one can approximately describe transitions as separately due to molecular translation, vibrations, and rotations, and electronic-state transitions. Of course, it is clear that this is rather approximate, with many exceptions and observable coupled events (e.g. vibronic transitions). If we can obtain a discrete-state description of our system, then we can use statistics (Boltzmann, Fermi–Dirac, Bose as appropriate) to find the partition function Z, and from it thermodynamic properties of interest. Then, if we have a mechanism for generating transitions between states, we can begin to model the dynamics of our system [3].

Linking both time scales is a deceptively simple-looking function referred to as the potential energy surface (PES); that is, the time-independent energy $E(\mathbf{X})$ of a system as a function of the vector of instantaneously frozen nuclear positions $\mathbf{X}$. The electronic state, total charge and possibly the stoichiometry of the system are additional parameters in a more generalized definition of the PES. Electronic motion is entirely encapsulated within $E(\mathbf{X})$; as we shall describe in more detail below, its accurate evaluation requires quantum mechanical methods in many cases; in others however, simple classical representations of $E(\mathbf{X})$—so-called atomistic models, casting electrons and nuclei into a single entity—are quite sufficient. In contrast, atomic motion is, for a vast majority of applications, sufficiently well approximated in classical terms; thus, we need not solve for the eigenfunctions of nuclear motion; instead we have to deal only with the far more accessible ensemble averages of N classical particles [4].

2.2. Beyond Born–Oppenheimer

Most of the following discussion is based upon adaptations of Hartree–Fock (HF) [5] and Density Functional (DF) [6] approaches which develop a one-electron self-consistent-field model; however, we must also take note of further lines of attack—such as Quantum Monte Carlo (QMC) and quasi-classical Reaction Dynamics [7] methods which incorporate more sophisticated electronic wavefunction data. Development of methods capable of extracting PESs and quantum transition-state information from ab initio wavefunction data is particularly relevant to the subjects of this review [8,9]. Applications to problems like the dissociative adsorption of hydrogen [10] and the adsorption and dynamics of water on MgO [11] can provide a valuable check on predictions of simpler schemes. The recent survey of QMC methodology and applications to solids by Foulkes et al. is very informative [12], and results for real materials such as bulk silicon show the rapidly growing range of applicability of these methods [13].

2.3. Back on the energy shell

Assuming that we have available to us a suitable representation of the PES $E(\mathbf{X})$—and we will discuss various realizations below-thermodynamic or ensemble properties can be extracted using a variety of techniques. In the rarest of cases where the system at hand is characterized by a single minimum on the PES, thermodynamic quantities such as the enthalpy, Gibbs free energy, etc. can be estimated via the vibrational eigenmodes and the standard expressions for an ideal gas; harmonic oscillator, rotating top, etc. Most 'interesting' systems have multiple minima and advanced methods of searching the configuration space are required.

Molecular Dynamics (MD) uses the calculated forces $\mathbf{F}_i$ of a configuration $\mathbf{X}$ to propagate it through phase space by integrating Newton's force-momentum equations

$$\mathrm{d}\mathbf{p}_i/\mathrm{d}t = \mathbf{F}_i = -\mathrm{grad}_i E(\mathbf{X}) \quad (1)$$

using discrete time-steps and some kind of thermostat to control the sample temperature. Simulation methods using classical equations of motion have turned out to be highly effective in addressing questions of dynamics and thermodynamics [14]. While fundamental electronic processes may occur in the femtosec (10^{-15} s) range, molecular vibrations are typically three orders of magnitude slower. The picosec (10^{-12} s) range of molecular vibrations generally sets the scale for time steps in atomistic simulations. The good news is that simple interatomic potentials can be found which adequately reproduce observed geometrical configurations, can be used to search for equilibrium structures, and are useful in describing transport and energy transfer over short time intervals [15–17]. The bad news is that with today's computers and straightforward algorithms, the available simulation time for a significant macromolecular or solid system is of the order of 10–100 ns. This is far less than required for study of diffusion processes and kinetics of many important reactions.

The Metropolis Monte Carlo (MC) method generates a stochastic ensemble in thermal equilibrium. Unlike MD it does not explicitly involve a time variable and it is often better suited to sample large regions of a configuration space with numerous local minima, which could not reasonably be explored in feasible simulation times. The key step in MC sampling is the generation of a Markov chain, a series of sequential random states of the system with a defined probability distribution

$$P(X_1,\ X_2,\ \ldots,\ X_N) = G[E(\mathbf{X}),\ T] \quad (2)$$

Depending on the applied constraints, the distribution $G(E,\ T)$ may be Maxwell–Bolzmann, or any other stochastic function optimized for the purpose at hand, such as employed in Generalized Simulated Annealing (GSA) [18]. GSA is a technique derived from MC which employs a variable temperature in order to survey large areas of configuration space either as a static method of identifying absolute minima or in preparation of constant temperature MC sampling [19]. Sequential or cyclic application of MC and MD techniques attempt to combine the advantages of both. It seems that a mixed procedure is rigorously justifiable, and offers an appealing way to treat groups of variables which respond on different time scales [20].

In the following, we will briefly discuss a number of schemes and their computer implementations-for the

sake of brevity an identifier is often given as (ACRONYM, program-name); details of implementation can be found in the cited references.

2.4. Finding $E(\mathbf{X})$

Of the various ways available to calculate the PES $E(\mathbf{X})$, first-principles methods are the most rigorous and accurate, since they are most closely formulated in terms of the fundamental laws of physics. Yet this 'closeness' comes at the price of computational cost. On the other hand, semiempirical approaches such as we sketch below maintain the formal structure of the quantum mechanical description, while introducing simplified expressions for the Hamiltonian and its matrix elements. When QM descriptions are still too complex or the size of the system is prohibitive, one resorts to a fully empirical (force–field) description of interatomic potentials.

2.4.1. First-principles methods

The single determinant HF model wavefunction, corrected by perturbation theory and/or limited configuration interaction (post-HF or HF^+) was long one of the cornerstones of quantum chemical theory [5]. Today it remains a useful variational tool, based upon the minimization of the energy of a single determinant wavefunction built from variationally determined spin orbitals. Its implementation and distribution in analytic Gaussian bases in programs such as GAUSSIAN, MOLPRO, CADPAC, GAMESS, CRYSTAL, etc. has been a major accomplishment in diffusing computational capabilities around the world. Both localized orbital (cluster) and periodic (band structure) implementations have been widely used. The main deficiencies of HF derive from the lack of correlation in the Hamiltonian (only parallel-spin exchange is included, partially corrected in HF^+), an incorrect or arbitrary treatment of excited states (correctable by a limited configuration interaction), and computational times which increase (in standard implementations) at least like M^3, where M is the number of basis functions. Nevertheless, with effective core potentials used to reduce the number of functions to be calculated, with extensions such as perturbative inclusion of spin-orbit effects, and computation of a variety of experimental properties, this methodology will continue to be usefully applied. Beyond HF, traditional quantum chemistry sets out a clear, if by and large impractical path for how to exactly include electron correlation into the model: full CI (complete configuration interaction), carried out at the basis set limit, promises those plentifully equipped with computing resources (and/or patience) the exact solution to the non-relativistic electronic Schrödinger equation. Impractical for all but the tiniest of molecular systems, necessitates the CI expansion be limited in one way or another: CISD, for example, forms a significantly smaller configuration space including all single and double excitations with respect to the HF 'reference' configuration. While this may adequately address correlation effects arising from interactions between one electronic state and another ('static correlation'), limited CI is a tedious approach when it comes to fully capturing 'dynamic correlation' that is, the instantaneous repulsion between pairs of electrons. Møller–Plesset perturbation theory (MPPT) to n-th order (MPn) as well as coupled-cluster theories (CCSD, CCSD(T) are common acronyms) offer a more direct representation of dynamic correlation; in turn, they pose difficulties in situations when static correlation effects become relevant.

The gradual unfolding of DF theory with its emphasis upon electron densities rather than the many-electron wavefunction, represents a second major direction of advance[21]. A starting point based upon a self-consistent procedure is developed which ultimately determines the ground state charge and spin densities, through solution of the single particle Kohn–Sham equations [22]. In practice, the resulting one-electron wavefunctions and eigenvalues have been extensively used to interpret both ground state and excited state properties. Rigorous prescriptions for the treatment of excitations have now appeared, and this remains an active area of development [23].

Use of periodic boundary conditions leads naturally to expansion of the DF wavefunctions in Bloch states, while chemically motivated localization concepts lead to finite-fragment cluster wavefunction expansions. Band structure technology has a very rich content; with the periodic potential and wavefunctions being represented in a variety of methodologies [24]. In an embedded cluster (EC) approach one chooses a finite localized fragment of the larger system, and solves the DF problem self-consistently in the density-dependent potential and boundary conditions derived from the host [25]. By moving around the 'window' which defines the local cluster, one obtains a sequence of views of the system, which can be patched together to represent the whole. The so-called Divide and Conquer (DC) scheme, which we describe in more detail below, places these ideas on a rigorous footing, and through the mechanism of a common Fermi energy (E_F, chemical potential) and provides a key for establishing equilibrium among the various clusters [26].

Developments in DF theory which have made it possible to expand the range of electronic structure analyses from that of moderate size ($N < 100$ atoms) molecules and periodic solids (here N is the number of atoms per unit cell) to that of macromolecules and defected/interfaced solids with thousands of atoms [26,27] are critical for obtaining basic data needed as input to semiempirical interatomic potentials. We com-

ment in some detail on one practical Order(N), or linear-scaling, approach—the DC scheme—to this problem in the following. Alternative efficient approaches have emerged, which take us back toward the initial 'dream' of solving the t-dependent Schrödinger equation. The development of 'Ficticious Quantum Dynamics' by Car and Parinello galvanized the field of first-principles MD, by simultaneously treating electronic and nuclear degrees of freedom with discrete time steps [28]. By treating the electron as a somewhat heavier particle, they were able to adopt a single $\Delta t \approx$ 1 fs in both electronic and nuclear coordinates. By using plane-wave (PW) representations of wavefunctions and DF (pseudo)potential and making use of fast Fourier transform (FFT) techniques, one gains significant computational speed. Furthermore, the use of PW's allows for rapid calculation of nuclear forces $\nabla_i E(\mathbf{X})$ at each time step by application of the Hellman–Feynman theorem. Successful applications have been reported for molecules, liquids, solids, and reconstructed surfaces [29–33]. Special procedures are necessary to keep electrons on their ground state energy surface, the so-called adiabatic solutions to the composite electron-nuclear state[34]. Implementation of gradient corrected exchange-correlation potentials in Car–Parinello total energy calculations brought 'chemical accuracy' of perhaps 2–3 kcal mol^{-1} to representations of relatively simple surface structures for which accurate pseudopotentials are available[35].

When electronic transitions become entangled with nuclear dynamics, it is necessary to consider nonadiabatic approaches; a relevant example would be the scattering, sticking, and surface diffusion of a molecule impacting upon a solid surface. A so-called Molecular Dynamics with Electronic Frictions (MDEF) scheme presented by Head-Gordon and Tully [36] which uses the Bohm formulation of quantum mechanics to recast the coupled Schrödinger equations offers such an approach. Taking a suitable classical limit, one obtains classical-like motion on each PES $E_n(\mathbf{X})$ associated with a particular electronic state 'n' accompanied by quantum transitions between the quantum states. This methodology is further described, and illustrated with simple examples and useful comparisons to other mixed quantum–classical approaches by Burant and Tully [37]. By parameterizing the first-principles data in the form of a friction tensor multiplying a velocity vector, plus a stochastic force to maintain the bath temperature, Tully et al. [38] modeled adsorbate vibrational relaxation of CO on Cu(100), and Springer et al. [39] modeled ultra-fast laser-induced desorption. We may expect to see further developments of this powerful approach.

While the formal content of DF theory continues to evolve, an equally important and concurrent development of practical computational algorithms can be observed. We focus in the following on the utility of EC approaches, and their use in realizing algorithms showing essentially linear growth, or Order(N), in computational effort with system size. Here N can be taken either as the number of electrons or as the number of atoms to be considered. There are a considerable number of ways to decompose a multi-atomic system to achieve Order(N) analysis times, dating back to the earliest days of computational physics and chemistry [40]. For example, the idea of partitioning the Hamiltonian matrix, given in a basis of atomic orbitals, appeals to basic ideas of chemical bonding and the limited range of interatomic interactions. Placing the resulting coupled equations in the language of Green's functions leads naturally to the concepts of embedding fields and accompanying boundary conditions, all of which can be subjected to reasonable approximations. Naturally, it would be desirable to avoid the calculation of wavefunctions entirely and to develop procedures which directly determine the density matrix [41]. Up to the present, such approaches have had limited success; however, the large potential payoff for a density matrix approach of chemical accuracy encourages further efforts. Efficient wave-function based DF pseudopotential (DF–PP) band structure approaches can be implemented exhibiting Order(N) behavior; recent progress is reviewed by Bowler and Gillan [42] and by Ackland et al. [43]. The VASP implementation of Kresse et al. has found extensive use for surface structures [44]. Even though DF–PP codes like VASP contain an O(N^3) matrix diagonalization, efficient programming permits treatment of large unit cells containing hundreds of atoms.

While PW expansion bases are convenient, and widely used in DF–PP approaches, they are notorious for their slow convergence—one would typically require thousands of functions for an accurate representation of solid-state wavefunctions. Thus, it is interesting to note demonstrations that localized spherical-wave expansions, offering many of the analytical advantages of plane waves, offer a more rapidly convergent basis with a sparse Hamiltonian matrix [45]. In variational calculations, whether with periodic boundary conditions or for ECs, the choice of basis is determined by a balancing of compactness of representation versus computational cost. Among the popular localized basis choices are analytical Gaussian-type (GTO), exponential Slater-type (STO), and numerical atomic orbital/atom in well solutions (NAO). Optimized representations can be obtained by mixing and matching- for example, plane waves plus GTO's; different classes of materials will obviously have different optimum representations.

Real space mesh techniques have the potential to replace the time-consuming generation of integral matrix elements by simpler difference equations, and in some approaches without the limitations of expansion bases. Beck has given an extensive review of progress in this area [46]; we may also cite the work of Fattebert and

Bernholc on optimized nonorthogonal orbitals and multigrid acceleration as one of the attractive evolving approaches [47].

2.4.2. Semi-empirical methods

Parameterized Hamiltonians and interatomic potentials are sought because of their unrivaled speed advantages. The use of semiempirical Hamiltonians to speed calculations and bypass limitations of first principles theory goes back to the beginning of computational chemistry, and includes methods with familiar acronyms like PPP (Pariser–Parr–Pople), EH (Extended Hückel), INDO (Intermediate Neglect of Differential Overlap), MINDO, ZINDO, SMNDO, AM1, PM3, etc. Commercial programs like MOPAC embody a suite of methods from which a knowledgeable modeler can make an optimum selection. Among the noteworthy recent developments is the successful incorporation of d-element parameterization, in the MNDO-d scheme of Thiel and Voityuk [48].

A noteworthy example of hybrid MD and electronic structure methodology is that of Tight Binding Molecular Dynamics (TB-MD). Tight binding schemes have a long and illustrious history in electronic structure theory, based initially upon the ideas of Linear Combination of Atomic Orbitals (LCAO) expansions in a minimal basis. Slater and Koster popularized TB-LCAO as a compact method for fitting first-principles band structures and adapting empirical band structures to experimental data [49]. On a more fundamental level, the fact that the Hermitian Hamiltonian matrix can be reduced to tridiagonal form leads to the idea of an optimal localized basis set with interaction of limited range. The resulting introduction and use of partial fraction expansions for quantities such as partial densities of states made the method both flexible and powerful [50]. Foulkes and Haydock showed that TB can be understood as stationary approximations to self-consistent DF theory, and gave prescriptions for calculating the required potentials and matrix elements [51].

More recently it was realized that with parameterized TB matrix elements representing electronic structure, time dependent problems could be solved for systems with thousands or millions of atoms with reasonable computation time [52]. In such cases a mixture of first-principles data and experimental constraints probably is most effective in forming the effective Hamiltonian. Some very nice recent examples include relations between magnetism and local order [53] and manifold thermo-mechanical properties of porous, amorphous, liquid, and solid Si [54–57].

2.4.3. Atomistic potentials

A parameterized interatomic potential must be sufficiently simple that it can be rapidly evaluated, and differentiated to produce atomic forces for simulations involving very many atoms over long timescales. At the same time it must flexible enough to adequately describe the material at hand; that is, it must be capable of reproducing what is already known, either experimentally or from first-principles calculations. However, flexibility of a potential on the other hand must remain balanced in view of how much is already known—a modeler whose potential has more parameters than input data is clearly up to nothing good. At the limit of extreme simplicity one finds short-range two-body interactions of the well-known Hooke spring, Lennard-Jones and Morse type, all with little effort evaluable at O(N) cost. The Coulomb potential between point charges is a simple two-body interaction; however, it is long-ranged and because of this its efficient evaluation at O($N \log N$) or even O(N) cost is somewhat more involved. Yet, with these simple potentials alone, quite capable models can be constructed, especially for systems that are typically ionic such as MgO. Molecular systems characterized by a significant degree of covalent bonding require additional three-body (angular) and four-body (dihedral) interaction terms in their potential models. Representations of metallic bonding in terms of two-body potentials have been challenging due to the perceived many-body nature of metallic cohesion; the widely used Embedded Atom Method (EAM) augments a traditional two-body potential with an effective many-body term $F(\rho)$ which is a function of the estimated local electronic density at the nuclear core [58]. The EAM has been successfully combined with first-principles DF energetics calculated for metal clusters to produce potentials which reproduce small particle structures and can perhaps be extended to bulk [59]. Recent approaches to improved representation of metallic bonding in atomistic simulations are reported by Deyirmenjian et al. [60], who further parameterize the dependence of potential energy upon local atomic volume.

One of the desirable features of atomistic potentials is some degree of transferability. The so-called Buckingham-type potentials

$$U(r) = Ae^{-r/b} - C/r^6 + q_i q_j / r \tag{3}$$

are widely employed in modeling ionic solids, and frequently used in conjunction with the 'shell model' representation of ionic polarizability. In this model the nucleus is attached by a spring to a rigid electronic shell, adding flexibility very useful in improving the description of electrical properties and resulting ion displacements [61]. In the case of oxides, Lewis and Catlow [62] and Gale and collaborators [63] have built up very valuable data bases. Gale's General Utility Lattice Program GULP has found many applications in predicting bulk and surface structures, using a periodic slab model with flexible potential parameters [64]. The

METADISE code permits one and two dimensional defect simulations allowing dislocations, surfaces and interfaces to be studied [65]; MARVIN is another example of a flexible periodic-potential modeling program [66].

Efforts continue to develop more accurate model potentials with only a few additional parameters. More elaborate transferable models for atomistic oxide simulations (applied to bulk Al_2O_3) were suggested by Wilson et al. [67], who found that both dipolar and quadrupolar contributions to the anion polarizability were needed to stabilize the corundum structure relative to bixbyite. They were able to rationalize this parameterization by observing the quadrupolar distortion of electron density around oxygen in PP-DF band structure calculations. Since this distortion is of rather short 'wavelength', they were able to observe improvements in the energy of the corundum phase as the plane wave cutoff was increased from 500 to 700 eV. Further developments toward obtaining a physically transparent and transferable compressible ion model for oxides are reported by Pyper, and Marks et al. [68]. By fitting a model with differential compressibility of oxygen 2s and 2p shells to correlation-corrected Dirac Fock data and to experiment on a single cubic phase of MgO, they were able to adequately reproduce experimental results for two additional cubic phases, and to show good transferability to the fluorite phases, such as ZrO_2. These results show that bulk properties can be reproduced precisely by atomistic models with a 'reasonable' number (10–15) of parameters, where adequate input data are available.

When one needs to introduce pairwise interactions which have not been previously 'calibrated', such as adatom-surface environments, it is convenient to use the simplest two- or three-parameter models such as the Morse potential,

$$V = D\{[1 - e^{-a(r-R_0)}]^2 - 1\} \quad (4)$$

Here the energy scale, equilibrium distance, and interaction range are completely transparent, and can be selected on the basis of analogy and intuition with some confidence. Iterative improvements are then possible, within a modest range of parameter variation.

Surfaces and interfaces present additional challenges for simulations of ionic materials, since reduced coordination and altered bond lengths in these regions lead to modified (generally reduced) atomic charges, as found in many ab initio studies. Considerable efforts have been made to find predictive models for variable charge; one of the more interesting chemically-based ideas is that of electronegativity equalization (QEq) introduced by Rappé and Goddard [69]. All the force-fields described so far are characterized by atoms of fixed charge. The QEq (charge equalization) method improves on this by permitting a degree of charge transfer between atoms. This involves an additional empirical expression for the electronic energy as a function of the atomic charges; typically, the atomic ionization potential and electron affinity enter into the parameterization of the electronic energy. For certain materials, a charge equilibrated model is far better equipped than charge static models to describe the often subtle interplay between geometry and charge distribution. The obvious alternative of calculating surface charges by DF methods can be carried out for scenarios like a low index surface of titania [70]; however, the results will be sensitive to details of surface relaxation and reconstruction, which may be beyond computational convenience or capacity. Inclusion of experimental surface data is one 'secure' method of producing a surface-ion charge parameterization [71]; however, such data are rarely available for doped, dirty, or interacting interfaces.

2.4.4. Cluster expansion method

A typical problem of oxide structure/thermodynamics and phase diagrams requires knowledge of the internal energy associated with a variety of site occupancies—typically involving a considerable number of defect configurations as well as local chemical composition in solid solutions like CaO–MgO. The cluster expansion method [72] provides a means of combining and counting the many topologically allowed arrangements to determine structural entropy, and from this the desired free energy versus composition. The 'interface' between thermodynamic approaches and methods for determining $E(\mathbf{X})$ is obvious, and some efforts to make the interfacing more automatic are being carried out, especially in the area of structural alloys [73].

The recent proposals of Fuks et al. for treating growth of metallic films on oxide substrates represent further steps to integrate electronic structures with thermodynamic approaches [74]. Using a so-called 'mixing potential' for an ensemble of occupied and vacant surface sites, they are able to develop a phase diagram (temperature vs. coverage) with inputs from HF^+ supercell band structure calculations (LCGTO-HF CRYSTAL). Their results for Ag/MgO(100) will be discussed in a later section. The maturity of finite-temperature first principles DF simulations can be seen in recent analysis of structure and dynamics at the aluminum solid | liquid interface [75].

2.4.5. Hybrid methods applied to $E(\mathbf{X})$

In strict interpretation, the term 'hybrid model' is often understood as the simultaneous use of quantum mechanical and atomistic techniques wherein parts of the system are treated quantum mechanically whilst others are represented using more approximate schemes; thus, the method of computation is smart in that the expensive quantum mechanical model is applied only in those regions that require them. The issues that arise are those of interfacing the two parts described by different

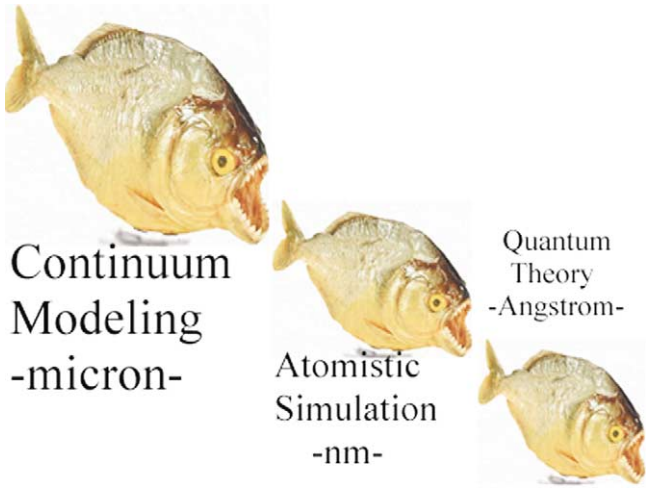

Fig. 1. A traditional top–down 'Food-Chain' view of time- and length-scale hierarchy.

models—one can consider serial, parallel, or mixed strategies.

Many viable implementations of so-called QM/MM (Quantum Mechanics/Molecular Mechanics) serial schemes have appeared [76]. Even though the basic ideas and algorithms are extremely simple, they already permit extraction of thermodynamic properties, diffusion rates, and micro-mechanical properties which can be compared with suitably constructed experiments. In addition, the MM schemes provide a natural bridge to the still-larger scales of modeling of macroscopic structures which may be based upon time- and space-adaptive finite element methodologies [77].

2.4.6. The third level-towards continuum modeling

The general topic of multiscale modeling extending into the continuum regime is very active at present, with the program of the recent International Conference on Multiscale Materials Modeling, held at Queen Mary University (London, [78]) representing a broad range of algorithms and applications. A hybrid mixture of continuum (typically finite element) and atomistic dynamics has been popular in studies of mechanics, fracture, and heat transfer in metallic systems for quite a few years. These techniques are now beginning to be applied with success first to semiconductors, and more gradually to insulating compounds. Fig. 1 shows a traditional view of the relationship between continuum, atomistic, and quantum levels of modeling; however, a more integrative view of interlinked processes now appears to be more appropriate.

3. One way to put the pieces together

From this point forward it is necessary to become more specific about computational schemes, time- and distance-scales, and target systems. It is also a good time to remember the cliché about the worthlessness of a quantum–mechanical description of a baseball game—at some point we need to extract the variables of interest, and suppress the underlying microstructure when it is not required. It will thus be important to think about schemes which can project Angstrom- and femtosec-scale data onto effective potentials governing nanometer- and nanosec-scale simulations, which in turn can inform larger scale continuum models. It is immediately clear that the data-flow has to be two-way; i.e. there have to exist effective feedback paths from larger to smaller scale to set boundary conditions and control the simulation scenarios, as indicated in Fig. 2.

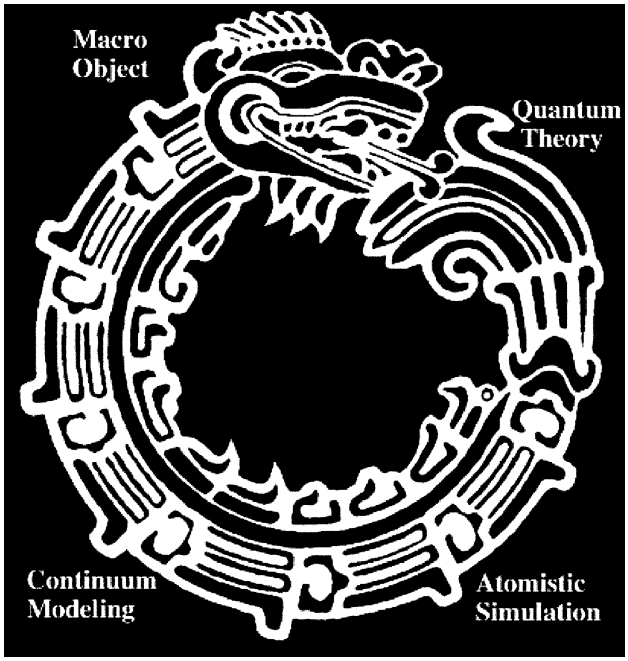

Fig. 2. A holistic view of data flow and interfacing between quantum mechanics, atomistic simulations, continuum mechanics, and macroscopic (experimental real world) components. Ouroboros is a recurring symbol among disparate cultures, representing unity, continuity, and integration; the graphic shown is from the Aztec civilization.

3.1. Coupling atomistic simulations and DF algorithms

Although we emphasize here the use of atomistic simulations as a 'search engine' for finding minimum-energy structures and mapping portions of the PES, the Embedded Cluster Density Functional (ECDF) scheme can also be used for this purpose. This is most effective when a rather small (<20) number of free structural parameters are to be varied, and we use atomic force algorithms already well-developed and tested for free molecules [79]. A few special precautions have to be taken to distinguish and utilize forces on well-described interior atoms, as opposed to those sensed by the overlapping buffer atoms.

In the present context we are most interested in the overlap and feedback between quantum mechanics and atomistic simulations. Consider the following scheme:

1) Generate a simple interatomic potential with parameters (U_1, U_2,..., U_M) optimized to fit some observed data—say lattice parameters, bond lengths, cohesive energy, and dielectric and elastic constants of a bulk crystal.
2) Create an (*hkl*) surface by cleavage of the ideal crystal, and 'decorate' with defects such as vacancies. Using the bulk-derived potential and MM, relax the surface structure to obtain coordinates (X_1, X_2,..., X_L).
3) Using the derived geometry, carry out DF analyses of surface and bulk regions. Extract charge densities, local atomic charges and bond orders (admittedly nonunique, but useful), binding energies and spectroscopic profiles.
4) Compare computed electronic properties with available data, and with theoretical data bases on related systems. Use these comparisons to improve the potential parameters (U_1, U_2,..., U_M) and repeat steps 2–4 until convergence in potential is achieved.
5) Use the optimized potential in simulations to predict diffusion and reactivity of the surface with incoming molecules, over the computationally available time interval. Pass this information on to the next coarser level of simulation, and back to DF procedures dedicated to description of the electronic structure associated with basic processes (adsorption, dissociation, recombination) of surface-molecule reactions.

In favorable cases, where there are few degrees of freedom the DF/classical interface can be organized to directly recover an effective interatomic potential [80]. In such a case where adequate atomic structural data are available, first-principles DF calculations can be effectively used to seek properties that can be fed back into atomistic models. The number of degrees of freedom is, however, too great to permit direct 'inversion' to obtain potential parameters. In addition we consider the value of projection techniques on electrostatic potential and charge distributions as a rapid-scan means of surveying interesting portions of the extended system. Further examples represent cases in which there exist some data (e.g. ideal bulk, impurity-free crystal) suitable for initial potential generation, but in which atomistic simulations play an essential role in determining local structures whose electronic properties are to be analyzed.

3.2. Divide and conquer-an Order(N) example

Among the various EC schemes, the DC method is a simple but clever generalization [26,27], drawing on the observation that a small cluster of atoms and some sort of representation of the surrounding material—yields at its central region or core an adequate representation of the local electronic structure. DC generalizes on this, by describing a large system patchwork-style by many overlapping clusters (see Fig. 3), each designed to yield within its core a representation of a subset (fragment) of the system at hand. Put differently, the density $\rho_A(\mathbf{r}; E_F)$ of a fragment A as it would be obtained in a traditional DF calculation on the entire system is approximated with that of the density $\rho_A^{\alpha}(\mathbf{r}; E_F)$ obtained when the DF equations are limited to cluster α of atoms involving the fragment atoms and a number of surrounding atoms (so-called 'buffer atoms'):

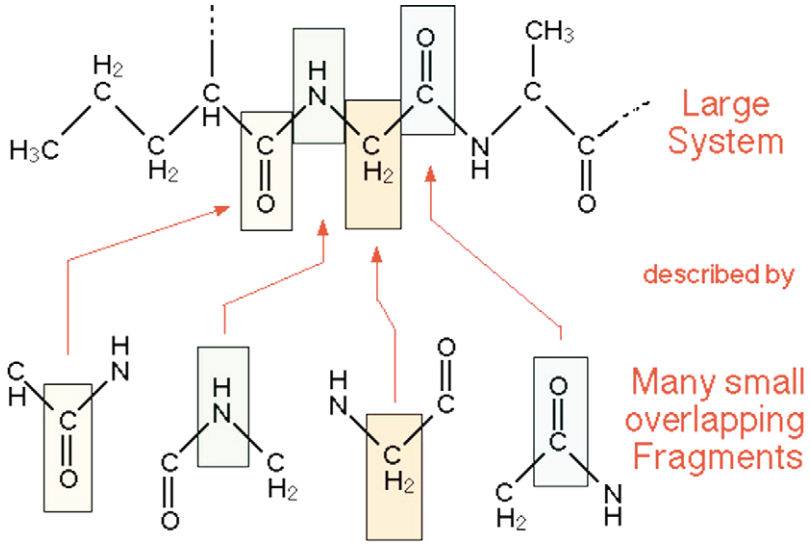

Fig. 3. Schematic of assembly of unique fragments to form extended structure in the divide and conquer method.

$$\rho_A(\mathbf{r};\ E_F) \approx \rho_A^{\alpha}(\mathbf{r};\ E_F) \quad (5)$$

Two points should be noted here:

1) The density is formulated here as parametrically dependent on the chemical potential or Fermi-level E_F, a quantity that is not known a priori. It is determined by the condition that the sum of densities of all the fragments that make up the system integrates to the total number of electrons; i.e.

$$\int \sum\nolimits_A \rho_A^{\alpha}(\mathbf{r};\ E_F) = N_e \quad (6)$$

2) A method of partitioning is employed in this process by which the density of a larger system can be split up into smaller parts; here, the density for the fragment is extracted from that of calculated for the cluster covering fragment- and buffer-atoms. The type of partitioning (Mulliken, space partitioning etc) is only of minor relevance provided the buffer is large enough and the partitioning is used consistently throughout the calculation.

With the Fermi level determined, the fragment densities $\rho_A^{\alpha}(\mathbf{r})$ calculated for all the clusters α are communicated between one another so that each cluster can appropriately update its embedding potential for the next cycle. This process is repeated until convergence in the density is accomplished.

How does this accomplish Order(N) behavior of computation time? As is well known, standard matrix diagonalization procedures such as are applied to a cluster of size M (measured by number of basis functions, $\sim$ number of atoms) have a M^3 characteristic resolution time. There are furthermore terms linear in M (generation of functions) and quadratric in M (assembly of potentials and matrices), so that time required for a single cluster behaves like $t_M = (a_1 M^1 + a_2 M^2 + a_3 M^3)$ with prefactors a_i that can turn out to be quite important. With fragments of constant size, the number of fragments P to describe the entire system is proportional to N and the computational time will be roughly $P\ t_M$; i.e. linear in N, and strongly dependent upon strategies for minimizing the typical fragment size M and efficiently passing data between parallel solutions of the fragment. Experience shows that this is indeed obtainable, even with the use of rather simple algorithms on loosely coupled multiprocessor networks.

From the self-consistent density and partitioned cluster wavefunctions, partial charges, densities of states and other electronic properties can be derived in much the same way as in traditionally performed DF methods. The accuracy of the DC is controlled by the size of the buffer of each cluster. Defining a buffer radius R_B, that is the distance from any fragment atom within which atoms are included as buffer atoms into a cluster, one can easily observe how calculated properties converge with respect to the buffer radius chosen. For certain properties where modest precision is adequate, such as partial atomic charges and densities of states, small cutoffs (e.g. $R_B = 5$ Å) often provide a good enough representation, allowing further acceleration of computations.

4. Applications to oxide surfaces and interfaces

The development and utilization of hybrid methodologies is driven by the complexity of real systems and the realization that no particular model provides a catch-all representation of the system. Only through collaboration between individually specialized methods, is a comprehensive understanding of the material at hand obtained.

Our present application examples pertain to metal oxide surfaces and interfaces, a subject which is far less simple than one might hope. It is a rich subject with a vast literature; in the following we pick and choose to illustrate power and limitations of currently used and evolving specific computational approaches and try to highlight the all-important interplay between them. We center and limit our discussion on the following five oxides:

1) Magnesium oxide (MgO, magnesia), perceived as a 'simple' oxide, being rocksalt structured and of high ionicity, often serves as the proving ground for new methods. It exhibits many of the typical properties of an oxide material, yet it reveals a rich chemistry of its own.
2) Sapphire (α-Al_2O_3, corundum), aside from its value as a gemstone, is used as an electronic substrate and in optical applications due to its large band gap and transparency, high dielectric constant, and hardness.
3) Titanium dioxide (TiO_2, titania) provides a third important case study: the interplay of two of its phases, rutile and anatase, is at the source of much of its catalytic activity. Its defect structure is central to performance (and degradation) as a base for paints and coatings, and as the main component of photohydrolysis solar-energy conversion cells.
4) Strontium titanate ($SrTiO_3$) exhibits interesting characteristics of a ternary compound with important electroceramic applications, and as a substrate for epitaxial overlayer growth. While not itself a bulk ferroelectric, it is a prototype of the host of important ABO_3 materials used in the electronics industry, and may exhibit useful surface ferroelectric phenomena.
5) Zirconium dioxide (ZrO_2, zirconia) is an important refractory structural ceramic (particularly in cubic,

Y-stabilized form), and due to its high oxygen mobility, used as in oxygen sensors and as a high-temperature electrolyte.

The field of applications presented to the modeler are equally manifold:

1) Surface reconstruction: Only in a few cases, such as MgO (100), do surface atoms displace little from their bulk positions. Most surfaces reconstruct and the preferred mode of reconstruction depends not only on the surface crystallographic plane but also on temperature and oxygen partial pressure at formation, to name but the most important. The modeler has to contend with the question of which of several possible surface layers has the lowest energy. Because of the multitude of possible reconstructions, collaboration with experimentalists is often warranted to narrow the scope; in turn present day experimental techniques are often barely able to resolve uniquely any but the simplest of surface reconstructions and theoretical models can help to fill the gaps.
2) Surface defects: It is often not the clean oxide surface that acts as a catalyst, but local imperfections, such as isolated or decorated vacancies, islands of surface overlayers, or the steps of high-index planes are generally the most potent areas.
3) Chemisorption: Adsorption and bonding of molecules on oxide surfaces has been studied intensively; however, detailed knowledge of site geometry is very limited, in contrast to the situation for pure metals and even semiconductors. Charging at the ionic surface and intrinsic surface roughness impedes successful application of many spectroscopic techniques, as well as topographical approaches such as Scanning Tunneling Microscopy (STM) and Atomic Force Microscopy (AFM). Thus theoretical studies can be of considerable value in developing surface-molecular structural models for comparison with experiment, once a certain degree of confidence in modeling of bare surfaces has been attained.
4) Surface reactivity: We consider examples of reactions which may take place upon an oxide surface in recognition of their wide use as catalysts and catalytic supports. For example, the reaction of water with an oxide surface and its resultant hydroxyl coverage is fundamental to the weathering of minerals, corrosion processes and catalyst/support properties.
5) Multilayers and overlayers: Artificial multilayer structures provide a tailored potential for electronic and optical resonators and waveguides, for spin-valve devices in magnetic recording and memory, etc. In order to produce multilayer films with controlled properties we must understand the atomic-scale structure at the interfaces.
6) Surface anchored structures: Finally, it is interesting to discuss further the role of oxides as supports for clusters and macromolecular structures which can be tailored for a highly selective function such as catalysis or molecular sensing. The scope of this field ranges from single dopant atoms, to few-atom clusters, to nanoparticles.

For the sake of convenience, we organize the following applications examples by material, starting with magnesia.

4.1. Magnesium oxide

4.1.1. Surface reconstruction

The phrase 'clean oxide surface' may be an oxymoron—for they are generally far from clean, and typically structurally more complicated than was initially believed, even for nonpolar surfaces of sodium chloride structures like MgO(001). The implicit large electrostatic fields of polar surfaces of magnesia like (111) are expected to cause near-surface charge transfers and reconstruction, which has been difficult to sort out experimentally. Many early efforts were focused upon atomically flat defect-free low index surfaces, with a small number of variable structural parameters. These parameters typically included interplanar relaxation δd_{ij} and rumpling Δ_i, defined as relative displacements of atoms about the mean plane.

Gerson and Bredow [81] give an excellent summary and comparison of results obtained for MgO by a multitude of schemes, including atomistic simulations, tight-binding and other semi-empirical models, HF and HF^+ as well as DF calculations. Each of the methods listed provides some of the elements required in a detailed analysis-putting these elements together is part of the task of hybrid methods. Atomistic simulations have provided valuable insights about the energetics of surface reconstruction, and give indications as to mechanisms of energy reduction for polar surfaces, which could hardly be obtained by direct electronic structure approaches. For example, Watson et al. [66] have shown that the MgO(110) surface should reconstruct to a zigzag microfaceted (100) structure, with a very considerable energy change from 3.02 to 1.87 J m^{-2}. Similarly, the polar MgO(111) surface apparently also reconstructs by facetting into non-polar (100) surfaces.

A good example of the distinct advantages of band structure approaches for reasonably simple or idealized periodic structures over EC schemes is the MgO(100) band structure reported by Towler et al. [82]. using a HF–LCGTO model. Nevertheless, as mentioned above, Gerson and Bredow studied MgO(100) with the semi-

empirical MSINDO EC model using an model of $8 \times 8 \times 4$ atoms and found surface relaxation geometries and energies not too much different from periodic DF models.

A recent proposal based on 'direct methods' refinement of surface X-ray diffraction (SXRD) data for the reconstruction of MgO(111) involves triangular arrangements of three oxygen atoms at close enough proximity to permit bonding; the structure is reminiscient of triangular ozone (O_3) which would certainly make for a rather intriguing mode of reconstruction [83]. However, as for most surface reconstructions, the experimental refinement of this reconstruction is characterized by a poor goodness of fit (poor in terms of what one would expect from bulk crystallography) and a confirmation of this structure by some other means is desirable. Theoretical modeling could provide such a confirmation. Starting with the experimental geometry, one could perform a relaxation with a method of choice: if the model finds a minimum close to the experimental structure, this would indeed be a confirmation of the structure; on the other hand, if the model relaxes significantly away from the proposed geometry then this would indicate that something is wrong, either with the experimental structure or the model. Whether this particular reconstruction of MgO(111) is real or an experimental artifact is, in our opinion still an open question, and nicely illustrates the point we are trying to make: this structure highlights the very limits of traditional (decoupled) atomistic models that have been so widely employed to rationalize MgO surface reconstructions. Unlike the popular (100) facetting reconstruction of the (111) surface, the proposed ozone-like reconstruction is non-stoichiometric; containing oxide anions in excess and thus requiring the presence of electron holes to achieve charge neutrality. We may with some confidence assume the holes are associated with the surface 'ozone-like' oxygen atoms; however, this then raises the question of how the underlying atomistic potentials of the electron-depleted oxygen atoms must change to reflect atomic configurations of the nonstoichiometric surface. One might suppose that further subsurface defect structures could arise to restore charge balance. The postulated structure simply falls outside the scope of decoupled atomistic models, and demands the application of hybrid techniques which are capable of generating geometry-dependent electronic densities and resulting $E(\mathbf{X})$ variation for different chemical scenarios.

4.1.2. Surface defects

With the advent of atomic-scale surface microscopy and accurate measurements of molecular adsorption and chemical reactivity, theoretical interest has moved toward description of defected and decorated surface structures. The manipulation of lower symmetry favors the use of ECs over periodic models. The greater number of structural parameters places increased computational demands on modeling of every type. For example, Ferrari and Pacchioni [84] carried out Gaussian-basis HF EC studies on the whole series of O and Mg surface vacancies—F_s, F_s^+, F_s^{2+}, V_s, V_s^-, V_s^{2-}, including oxygen vacancies at edge sites. Although the results suffered from the usual HF problems of omitted correlation effects, limited basis freedom, embedding problems (point charges, with variational clusters such as $Mg_{21}O_{20}$), limited capacity to carry out geometrical relaxation, etc. they pointed the direction to future systematic studies on a group of related structures within a chosen methodology. Scorza et al. [85] reported a number of improvements in this general framework, including improved embedding (external ions represented by a pseudopotential, three layer infinite slab), estimates of electron-correlation beyond HF through Møller–Plesset to second order (MP2), partial optimization of basis sets, and more extensive treatment of neighboring ion relaxation. Their results on F_s centers, obtained with the EMBED code, could be compared more or less directly with those from the related band-structure code CRYSTAL, as reported by Orlando et al. [86] It further occasions a comparison with the DFT band structure study on the neutral F_s center of Kantorvich et al. using core pseudopotentials and a plane wave expansion [87].

Ojamäe and Pisani considered the formation of divacancies at the MgO(001) surface, using HF EC methods with an LCAO Gaussian basis, embedded in a perfect crystal slab [88]. This is a nice example of use of the EMBED program suite, in which local relaxation of atomic positions (here first and second neighbors, depending upon cluster size) is included. Both neutral and singly charged (electron trap) divacancies called pit (V_{Mg} at surface, V_O directly below) and tub (V_{Mg} at surface, V_O as surface nearest neighbor) were considered; the tub configuration was found to be favored. Neighboring ion displacements of ~ 0.2–0.3 a.u. were predicted. A very large complexation energy of 300 kcal mol^{-1} was found in comparison to isolated charged defect pairs.

Gianello et al. extended analysis of isolated oxygen vacancies V_O at the MgO(001) surface, giving an interpretation of the paramagnetic F_s^+ and F_s^+ (H) sites believed to be associated with an electron trapped at V_O, and associated with a nearby proton, respectively [89]. Their methodology consisted of HF treatment of small clusters $(O_nMg_{n+1})^+$ embedded in an array of $\pm 2e$ point charges, and was used to differentiate between defects located on flat facets and edges and steps. Comparison of calculated spin densities with EPR led to the conclusion that flat facets were favored; however, a number of competing models and uncertainties remained, particularly concerning transient behavior.

D'Ercole et al. returned to this subject with a higher level of sophistication, modeling H_2 dissociation in the presence of V_O in an EC HF (EMBED) approach [90] with improved basis sets, a four-layer slab, pseudopotentials, etc. Significantly, the results, primarily that the isolated surface anion vacancy is probably excluded as the formation site of the F_s^+ (H) center, are quite contrary to those of previous cluster models [91–94].

One is reminded of the Pauling Point fable, in which a plot of 'theory' versus 'time' oscillates about the base-level value 'experiment' with amplitude which, hopefully, decreases with time. Pauling Points consist of zero crossings; i.e. excellent agreement with experiment. Considering the high mobility of hydrogen, it seems likely that a dynamical treatment, such as ab initio MD would be an attractive next choice of methodology. In the meantime, Soave et al. extended the methodology further using the program suite GAUSSIAN to treat relaxation more completely, and to introduce some degree of correlation effects [95]. DF approximations (B3-LYP and HF-LYP) to correlation were added in a HF^+ analysis of reactions $F_s^+ + X_2 \rightarrow F_s^{2+} + X_2^-$ for X = O and N, giving a rather satisfactory account of a variety of experimental facts.

The somewhat more exotic adsorption of atomic oxygen on the MgO(100) surface was considered (DF–PP) by Kantorovich et al. [96]. This model has a clear relation to questions raised in the discussion of ozone-like surface teminations discussed above. Its experimental significance remains to be clarified.

4.1.3. Molecules on surfaces

FTIR spectroscopic and DF cluster model (LCGTO-DF) studies of methane adsorption on MgO(100) carried out by Ferrari et al. gave a consistent picture of a weak interaction, with CH_4 preferentially bound at low-coordination ionic sites [97]. Point-charge and pseudopotential-ECs ranging in size from Mg_4O_4 to $Mg_{12}O_{12}$ were considered, with gradient corrected exchange-correlation potentials. Theoretically determined vibrational frequencies were found to be in qualitative agreement with FTIR data, with substantial relaxation of binding-site ions predicted. Coordination to corner-site Mg^{2+} was found to be most favored. Co-adsorption with CO was also used as an experimental diagnostic of site preference; however, no corresponding calculations were reported. Energetics of NH_3 adsorption at the MgO(001) surface were studied by Pugh and Gillan [98] by the DFT–PP technique.

Using photoemission and X-ray standing wave techniques Liu et al. found that the hydroxylation of MgO(100) takes place in two stages: at low vapor pressure H_2O dissociates at defect sites forming 5–10% monolayer (ML) coverage, and at somewhat higher pressure also interacts with terrace sites leading to a 50% ML product[99]. Exothermic reaction with corner and edge sites was indeed predicted from semiempirical (MSINDO, parameters optimized on gas phase molecules) cluster studies [100]; however, terrace-site bonding was found to be unfavorable, suggesting the importance of thermodynamic factors at the 'high' pressure of 10^{-4} Torr.

Surface reactivity can be probed and altered by atomic deposition. Abbet et al. decorated MgO(100) with $\sim$0.01 ML of Pd atoms, using a soft-landing impact method which permitted isolated atoms to diffuse over the surface to low energy binding sites [101]. Monte Carlo simulations proved helpful in predicting that most metal atoms would be isolated, thereby forming the simplest possible controlled reaction sites for incoming molecules [102]. Analyses by thermal desorption spectroscopy (TDS) and Fourier transform infrared spectroscopy (FTIR) were compared with gradient-corrected DF cluster models (GAUSSIAN method, as described above) to infer that Pd traps at defect sites, which are probably F_s and F_s^+ centers. The cluster calculations suggest the existence of an 'atop' CO–Pd geometry, with Pd–surface plane distances ranging from 1.94 Å for a F_s terrace site to 2.37 Å for an oxygen terrace site. Both Pd(CO) and $Pd(CO)_2$ complexes were predicted to be stable, with some experimental evidence of the dicarbonyl. $Pd(CO)_3$ was found to be unstable with respect to dissociation into dicarbonyl and gas phase CO—thus suggesting that the DF cluster approach, in its elaborated form, is capable of quantitative predictions of surface-adatom-molecule interactions. Some renormalization of computed properties, such as CO vibrational frequencies, is still required, but a consistent and coherent description emerges. In a similar approach (LCGTO-DF, PARAGAUSS) it was suggested that single Pd atoms attached at electron-donor sites would be capable of carrying out the acetylene cyclotrimerization reaction $3(C_2H_2) \Rightarrow C_6H_6$; however, neither transition states and activation barriers, nor reaction paths were investigated [103]. It is worthwhile to mention here the study of Yamauchi et al. on interaction of Pd_3 clusters with MgO(100) in an isolated small cluster model ($Pd_3Mg_8O_8$) in the LCAO-DF (DMOL) scheme [104]. As they did not treat adsorption on the defect sites believed to be key to surface–molecular interactions, and no details of charge transfer to/from Pd were presented, the main results of interest concern predicted $Pd_3 \Rightarrow Pd_2 + Pd$ dissociation energy, and preferred surface stacking arrangements.

Subsequently, Abbet et al. carried out experimental and theoretical studies of CO oxidation on single Pd atoms supported on MgO(100) [105]. Using the hybrid Born–Oppenheimer local-spin-density molecular dynamics (BO-LSD-MD) scheme [106] they were able to identify $Pd(CO)_2O_2$ and $PdCO_3(CO)$ as surface-bound precursors associated with observed low- and high-temperature reaction channels, respectively. This meth-

odology employed scalar-relativistic pseudopotentials, GGA corrections to energies, and a point charge embedding model. Constrained energy minimizations located the transition states, from which the CO_2 desorption was followed by microcanonical MD simulation. Thus, many fine details of the reaction dynamics are predicted, including the division of energy into translation, vibration, rotation, and chemical bond reorganization. Evidence is presented to suggest the migration of remnant Pd–CO fragments to form dimers and ultimately larger metal clusters.

4.1.4. Interfaces

Beyond the context of our 'simple' MgO examples, we note the extensive use of MgO films in ac plasma display panels. Here the films play a dual role as protectors of dielectric layers and as secondary electron suppliers, with deleterious effects of direct contact to the plasma being found as erosion, surface contamination, and changes in density and surface topography. Lee et al. [107] studied e-beam evaporated MgO films deposited on Si, which were found to have a [111] preferred orientation, using variable-incident-angle optical ellipsometry to measure variation of properties with depth. Using a multilayer model with variable dielectric properties and void fraction, they found their films to consist of a dense interface layer next to Si, a porous middle layer, and a roughened surface layer. The porosity and roughness has strong implications for adsorption of water, density of bound hydroxyl groups, and oxygen diffusion through the films. The inferred layer thicknesses (top: 17–31 Å, middle: 396–558 Å, interface: 20–37 Å, depending upon deposition conditions) delineates the nanoscale challenge to detailed modeling which this system presents.

The interface properties of MgO further play an important role in mineralogy, specifically through the weathering and dissolution of brucite ($Mg(OH)_2$) and periclase (MgO). Scanning force microscopy (SFM) of surfaces undergoing erosion under controlled pH show retreat of micro-steps at the edge of nearly square pits, with heights up to 120 nm [108]. A model was proposed in which the (001) surface is restructured into (111) nanofacets which are stabilized by protonation reminiscent of the bare facetting models discussed above; an idea which could now be checked by detailed atomistic simulations in acidic solution.

Another interface of practical interest, which complements the preceding examples, is that of the Fe–MgO–Fe system with demonstrated giant magnetoresistance properties. Surface X-ray structure analysis of 1–2 ML of epitaxial MgO deposited on Fe(001) suggested a regular stacking of oxygen atoms above Fe, and Mg atoms in four-fold hollow sites, with a slight rumpling (0.2 Å) within MgO layers, and interatomic distances as expected from ionic radii and the bulk lattices [109]. In contradiction to this picture, Meyerheim et al. found that ultrahigh vacuum deposition by electron evaporation led to an intermediate FeO layer between MgO and Fe(001) [110].

DF band structure calculations by Butler et al. on ideal Fe | MgO | Fe interfaces suggested magnetoresistive enhancements $\Delta R/R > 10$, highly dependent upon the overlap of propagating states in Fe and evanescent states in the MgO layer [111]. Since recent experiment (see above) indicated the presence of a buffer layer of FeO, one may have a reason for the observed much smaller $\Delta R/R$ and a direction for future modeling.

Using a combined thermodynamic, ab initio electronic structure approach, Fuks et al. studied the growth mode of silver on MgO(100), in an idealized model with no surface defects [112]. Considering (2×2) extended surface unit cells with three- and five-layer slabs, they were able to explore coverage ranging from 1:4 to 1:1, finding that Ag prefers to bind above oxygen. Computed energies per lattice site for highly symmetric configurations were used as input to a mixing potential model, which was used in turn to generate the 2D phase diagram for varying silver coverage versus temperature. With a calculated O- to O-diffusive barrier of only 0.05 eV, Ag is predicted to be highly mobile even at low T, leading to fast aggregation to a 3D island structure at room temperature, consistent with observations. It would be very interesting to augment these static/thermodynamic analyses with surface diffusion and growth simulations based upon the same potential data. This is clearly a situation where no single $E(\mathbf{X})$ surface is appropriate, and where a variety of scenarios could be explored in parallel.

4.2. Alumina (α-Al_2O_3, corundum structure)

A second 'classic' material preferred for surface studies is sapphire or α-alumina, Al_2O_3, prized for its hardness, transparency, refractory character, large bandgap and dielectric constant and as a substrate for surface overlayer growth. While other alumina phases are important as catalytic supports, their surfaces are much more difficult to characterize and we focus here only upon the simplest case where, for example, relaxation of the (0001) surface can be measured and modeled [113], as well as other low energy faces such as $(01\bar{1}2)$ [114] using band structure and EC DF methods, respectively.

4.2.1. Surface reconstruction

For α-alumina there may exist oxygen- or metal-terminated surfaces, depending upon preparation conditions as well as relative energetics [113,114], and upon which adsorption takes place or overlayers may be grown. Structure and energetics of the (0001) surface of α-alumina were investigated by Manassidis et al. via DF

pseudopotential calculations [115], and later extended to other low-index faces [116]. As evidence of continued interest in high quality models of the (0001) surface, we cite the periodic supercell [DF-PP plane wave] results of Batyrev et al. [117], who carried out relaxation studies of five different terminations. This work is especially notable in that a procedure for determining surface energy as a function of oxygen excess and oxygen partial pressure pO_2 was developed and tested.

4.2.2. Molecules on surfaces

The overwhelming number of experimental and theoretical studies of molecular adsorption upon alumina are concerned with interactions with metallic atoms or particles previously deposited, due to the catalytic implications. These studies, while important, throw little light upon fundamental surface-molecule reactions which are themselves of interest—for example, the consequences of water and hydroxyl adsorption on fine alumina particles in the atmosphere from solid rocket exhausts. Fortunately, theoretical and experimental analyses of adsorption upon 'native' alumina surfaces are beginning to appear; Hass et al. report extensive Car–Parinello supercell and DF cluster calculations on the Al-terminated (0001) surface with differing levels of H_2O coverage [118]. They find, not surprisingly, that the previously studied $(Al_8O_{12})H_2O$ and similar cluster models used by Wittbrodt et al. [119] are not very reliable for site relaxation and energetics determination. Strong influence of hydroxyl coverage for controlling deposited metal dispersion and growth morphology for Cu on the (0001) surface was proposed by Jennison and Bogicevic, making use of the (VASP) DF-PP supercell methodology [120]. DF cluster calculations continue to be useful in exploring more complex surface-molecular structures, such as isocyanate [121] and silyl esters [122] on α-alumina and methanol on γ-alumina [123].

4.2.3. Interfaces

For electronics applications, growth of metal overlayers is particularly interesting; Gomes et al. have modeled the initial stages of Pd growth upon the (0001) surface [124] by both EC (GAUSSIAN, CRYSTAL) and periodic (VASP) DF methods. First principles calculations of the ideal cleavage energy of bulk niobium Nb(111) | α-Al_2O_3(0001) interfaces were reported by Batirev et al. [125] by periodic supercell (DF-PP, plane wave) methodology. They demonstrated that lateral relaxation of anions not previously considered is of considerable importance in determining relative interfacial energies, and that this also has perceptible effects upon interplanar relaxations.

4.3. Titania TiO_2

Titania, TiO_2, is used in huge quantities as a basis of white pigments in paint, as a catalyst support medium, and as a gas sensor element. Its photochemical behavior and reactivity is in large part due to the presence of defects, primarily oxygen vacancies.

4.3.1. Surface reconstruction

(110) oriented TiO_2 crystals show three different surface terminations; the bulk (1×1) truncation, added rows of stoichiometry Ti_2O_3 to produce a (1×2) reconstruction, or added rows of TiO_2 to form a different type of (1×2) with cross-links. It has been found that the (1×2) reconstructions show different reactivity toward oxygen at elevated temperature and a model for the structure of the rows and cross-links has been proposed. For large departures from stoichiometry, defects can cluster and form crystallographic shear (CS) planes within the crystal in which adjacent regions of the crystal are displaced half a lattice unit in the direction with respect to each other. On TiO_2(110) such shear planes have recently been shown to terminate at the surface in a well ordered array of half height steps [126]. Early cluster DF calculations by Onishi et al. correctly identified the (1×2) rows or strands of Ti_2O_3 composition [127]. Pseudopotential DF band structure calculations performed by Lindan et al. on TiO_2(100) 1×3 reconstruction [128,129] and spin polarized calculations on reduced and reconstructed TiO_2 (110) surfaces [130] helped to develop both qualitative notions and quantitative data on ionic charge states and bonding. More recent DF band calculations by Li et al. established the structure of surface pseudohexagonal 'rosettes' [131]. Swamy et al. have generated variable-charge models for MD simulations of (100) [132,133], (001), and (110) [134] rutile surfaces, with the aim of attaining a degree of transferability, using the electronegativity equalization QEq model to obtain surface-variability of ionic charges. In this case MD simulation results, previous simulations, experimental SXRD and a variety of HF and DF calculations have been compared, giving a rarely available overview. It was noted that experiment and first principles theory agree rather nicely as to structural relaxation; however, the empirical simulations differ considerably among themselves and with experiment. Unfortunately, the effective potential using QEq model charges fares no better than others; the authors suggest that surface charges are underestimated by the model. The presence of low frequency surface-localized vibrational modes is pointed out as a possible cause of some remaining discrepancies between SXRD and HF/DF theory. Calculated surface formation energies show considerable scatter- once again the several HF/DF predictions are in general agreement on relative ordering: $(110) < (100) < (001)$ while differing

up to ~30% in absolute value. Unfortunately, the variable-charge force field models show greater variation, and sometimes predict incorrect ordering.

Extensive SRXD analyses for TiO2(110) have been reported, which are in fairly good agreement with O^+ ion-scattering data; however, 'experimental' relaxation displacements differ somewhat from each other, due to both data limitations and different modeling schemes used [135,136]. Generally speaking, the displacements predicted from first principles calculations [137–139] are small and less than those inferred from experiment. The surface-relaxation predictions of Ramamoorthy et al. [137] show good overall agreement for Ti positions with the SRXD data, but show bridging-O inward displacement only 1/4 that of experiment. As pointed out by Bates et al. [140], the calculations and experimental measurements do not refer to exactly the same quantity. The calculations give results for relaxed nuclear positions, whereas the X-ray diffraction experiments probe the electron density distribution. At the same time, the unrelaxed TiO2(110) surface was used in the theoretical simulations of STM experiments at rutile surfaces, and a good interpretation for STM images was obtained [141].

4.3.2. Molecules on surface

Hydrogenated rutile (TiO_2) is of considerable interest, due to its potential in photochemical cleavage of water [142], while adsorption of molecular nitrogen is interesting from the point of view of atmospheric processes [143]. Sodium adsorption provides another opportunity to compare theory and experiment [144], with hopefully simplified ionic interactions. The most important surface reaction of titania is probably that of water, due to its potential use in photocatalytic hydrolysis with huge implications for the energy economy. First principles MD simulations (DF-PP) of water adsorption and dissociation on TiO_2(110) were reported by Lindan et al. [145,146].

Bennet et al. observed the adsorption and decomposition of formic acid on (1×2) non-stoichiometric TiO_2 surfaces [147], while Ameen and Raupp used IR spectroscopy to study photocatalytic oxidation of airborne *o*-xylene and methylamine by titania [148]. These are excellent subjects for hybrid modeling, in the context of the known strong dependence (including blue coloration) of surface reactivity to nonstoichiometric selvage composition. Stone et al. carried out STM and AES studies of Pd on TiO_2 [149]. Further STM studies by Diebold et al. showed that surface properties of rutile (110) depend strongly upon the state of bulk reduction under various conditions, including annealing in oxygen, decoration with Pt clusters, and with adsorbed sulfur [150] The observed mixture of nano- and mesoscopic surface features is clearly related to diffusion of bulk defects, with consequences for macroscopic properties such as the conductivity changes exploited in gas sensors. Such observed features as encapsulation of Group VIII metals, and formation of the sulfide phase provide suitable challenges for theoretical modeling.

4.3.3. Interfaces

The initial stages of growth of metal overlayers can proceed by nucleation of islands or rafts- which may either grow outward to form uniform layers, or pile up to form 3D balls or mountains which try to minimize contact with the oxide. Theoretical studies of initial growth mechanisms can be useful in designing deposition conditions. The bonding structure and binding character for the initial stage of thin film growth of Ni on a rutile (110) surface was studied by Cao et al. [151], using the Discrete Variational (DV) EC scheme. This surface has an open structure, where coordinatively unsaturated oxygen and titanium atoms make ridges and ditches, respectively, along the [110] azimuth. The six uppermost oxygen atoms, called 'bridging' here, are of especial interest as interaction sites, while secondary surface oxygens form walls of the ditches. The Ti environment consists of rows of six-fold coordinated sites covered or protected by bridging O, and by rows of five-fold sites lining the ditches. Adsorption of Ni on the rutile surface will likely tend to restore oxygen positions toward bulk values, but with reduced local symmetry. On this basis, Cao et al. adopted the unrelaxed TiO_2(110) surface model, varying only position of the adatoms within a stoichiometric neutral cluster of composition $Ti_{15}O_{30}Ni_x$. They first examined single Ni atom adsorption, considering seven possible adsorption geometries: (A) on top of five fold surface Ti; (B) on the bridge site between two secondary oxygens, (C_1) on top of bridging oxygen, (D) three fold sites which consist of two secondary- and one bridging-oxygen, (E_1) on top of secondary oxygen, (F) on the four fold site between oxygens, and (G) on the three fold site which consists of two bridging- and one secondary-oxygen (see Fig. 4).

It was found that all the Ni-adsorption sites near oxygen atoms are favored over the Ti-atop position, and the oxygen-atop sites are most stable. The binding energy on bridging O atoms is only a little larger than that on the non-bridging surface O. The Ni–O bond lengths are 3.33 au and 3.12 au, compared with 3.82 au for NiO bulk; the binding energies are 4.42 and 4.72 eV for sites E_1 and C_1, respectively. It is noteworthy that, except for the atop-Ti case, which shows a weak Ti → Ni electron transfer, electrons transfer from Ni to the substrate. The net transfer is much less than one electron in every case, ranging over 0.2–0.3*e* for singly adsorbed atoms, and somewhat less for Ni_2 dimers.

The interaction energy between two adsorbed Ni at nearby surface sites was calculated, and the changes of electron transfer compared with a single adsorbed Ni. The interaction energy is defined here as $E_{int} = E_d - (E_{d1} + E_{d2})$, where E_d is the binding energy of two

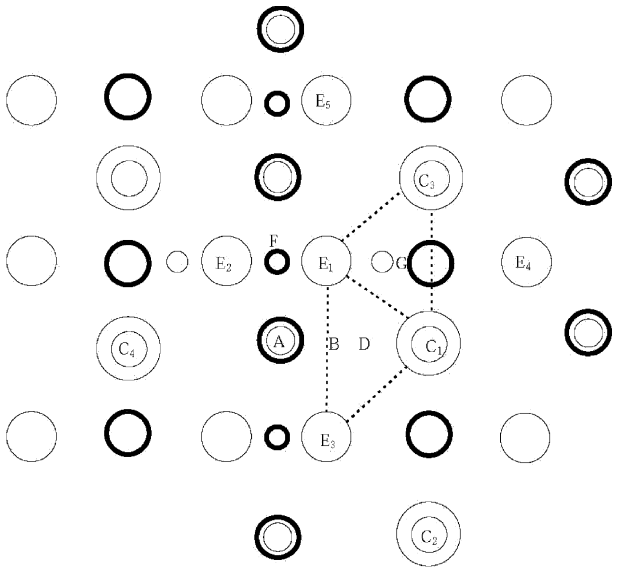

Fig. 4. Top view of TiO_2 (110) surface, showing Ni adsorption sites [151].

simultaneously adsorbed atoms, and E_{d1} and E_{d2} are the binding energies of the two atoms as they are adsorbed separately, at the same sites. Attractive interactions between the nearest-neighbor adsorbed Ni were found; the maximum attractive interaction energy being 2.10 eV between sites E_1 and E_2, which are separated by a distance of 4.78 au. For a free Ni_2 molecule, the experimental binding energy is 3.64 eV and the equilibrium distance is 4.23 au [152].

Thus, considering that the charge transfer between surface-bound Ni atoms and substrate is very small, the calculated interaction energies for the Ni dimer on TiO_2 are quite reasonable. The interaction energy of 1.04 eV per Ni atom on E_1 and E_2 sites is still much smaller then the binding energy of 4.42 eV per Ni atom on these sites; i.e. the Ni–O interaction dominates over Ni–Ni by a factor of four. At large distance, the interaction between two adsorbed Ni atoms is clearly through the electrons of the substrate surface, and not through the direct overlap of Ni valence orbitals. As the distance between adsorbed Ni atoms increases, the predicted interaction energy decreases rapidly, with some repulsive interactions observed, being understood qualitatively in terms of the Friedel oscillations of the indirect substrate-mediated Ni–Ni interaction.

Thus, for first layer Ni, the bonds between Ni atoms and substrate are rather strong, and much stronger than bonds between Ni atoms. The preference of Ni atoms for binding to substrate (on top of two kinds of oxygen atoms) rather than to other Ni atoms, thus leads to the complete coverage of the first monolayer of Ni deposited on the substrate, in agreement with Auger intensity experiments, where the break points for the Auger O(KLL) and Ti($L_3M_{23}M_{23}$) spectra appear at almost the same place, i.e. 4.72 au depth. Since the Ni adatoms in the first monolayer are locked on the top of the oxygen atoms in an array incommensurate with bulk Ni, no new long range order will appear as Ni is deposited, up to some critical thickness.

4.4. Strontium titanate, $SrTiO_3$

4.4.1. Surface reconstruction

Recent ab initio calculations of perovskite-structured $SrTiO_3$(100) (STO) surface relaxation for the two different terminations (SrO and TiO_2) analyzed their electronic structures (band structure, density of states, and the electronic density redistribution with emphasis on the covalency effects). Results of HF^+ models with electron correlation corrections and DF theory with different exchange-correlation functionals, including hybrid (B3PW, B3LYP) exchange techniques were compared. The results are also compared with previous ab initio PW local density approximation calculations and experiments. Considerable increase of Ti–O chemical bond covalency nearby the surface and the gap reduction, especially for the TiO_2 termination, were found [153,154]. Cheng et al. studied structural relaxation and longitudinal dipole moment of $SrTiO_3$(001)(1 × 1) surfaces [155], using the DF-PP methodology.

For the (001) surface of $SrTiO_3$ alone, LEED, RHEED, STM, and SXRD studies have revealed numerous reconstructions: (1 × 1), (2 × 1), (2 × 2), c(4 × 2), c(6 × 2) and ($\sqrt{5} \times \sqrt{5}$)R26.6° [156]. Considering how very little is known about the exact atomic arrangements in these reconstructions, owing to the considerable experimental difficulties of surface diffraction, theoreticians certainly have got their work cut out for them. With the –SrO–TiO_2–SrO–TiO_2– stacking order in ⟨001⟩ direction, two alternative surface-terminations are with the TiO_2 layer or the SrO layer: For the smallest of the $SrTiO_3$ (001) reconstructions, the (1 × 1) surface, a number or first-principles studies have been reported. The earliest electronic structure calculations on the $SrTiO_3$ surface employed cluster methods, performed at positionally unrelaxed surfaces; Wolfram et al. [157] employed an empirical LCAO method and Tsukada et al. [158] used DV-Xα cluster calculations to identify surface states. Kimura et al. [159] have applied PW pseudo-potentials method to the TiO_2 terminated surface and studied the effect of oxygen vacancies on the surface electronic structure. With modern periodic, PW and/or GTO-HF codes, geometry optimizations have now become possible. Vanderbilt et al. [160] employed the PW pseudo potential method to relax the atomic positions for the SrO and TiO_2 terminated surface. Kotomin et al. compared the results of GTO-based DFT and HF^+ calculated surfaces relaxations and find good agreement between the various functionals used [161]. In detailed discussions of the electronic structure,

they find through bond-analysis, increased covalency near the surface for both the TiO_2 and the SrO terminated surface.

If very recent direct methods refinements of SXRD data [162] are to be believed though, at least some $SrTiO_3$ (001) surface reconstructions—the (2×1) and $c(4 \times 2)$—are characterized by an additional TiO_2 overlayer on top of an already TiO_2 terminated surface (Fig. 5). Well, nobody said that surfaces reconstruct stoichiometrically; Nature certainly did not. This too highlights in our view the continued need for hybrid methodology. Whilst one can only be impressed by the capabilities of modern electronic structure codes regarding their ability to perform structural optimization, we are still far from be able to predict surface reconstruction ab initio.

Even for a material of a comparatively simple composition and unit cell, such as $SrTiO_3$, there are simply too many variables to consider. What is the reconstruction cell? What is the surface stoichiometry? These are both questions that need to be addressed before one may even begin thinking about how the atoms are actually positioned. This necessitates the use of much faster empirical methods in order to more efficiently narrow down the number of possible structures. Various atomistic (shell-model) simulations on $SrTiO_3$(001) have been reported [163,164], which are generally characterized by (perhaps questionable) assumptions of stoichiometric and minimal reconstruction scenarios.

4.4.2. Molecules on surfaces

Perhaps because clean STO surfaces have only recently begun to be characterized, relatively few theoretical studies of molecular adsorption have been reported. Torres et al. have carried out HF supercell studies (GTO-CLUSTERD) of chemisorption of water on (001) surfaces for both cubic and tetragonal lattices[165]. Stashans et al. have used the same methodology to examine oxygen vacancy | O_2 interactions on the same surface [166]. Abundant experimental data are now beginning to appear, which should stimulate modeling directed toward potential catalytic activity and formation of electronically active interfaces. For example, reduction of methanol on $SrTiO_3$(110) followed by desorption has been characterized by Yoshikawa and Bowker [167], and adsorption sites of precursor molecules, (such as CH_4, akylsiloxanes) in CVD processes and in self-assembly of ordered films on (Ba,Sr) titanate (100) SrO surfaces have been reported [168,169].

4.4.3. Interfaces

Understanding initial formation and growth of metallic overlayers on $SrTiO_3$ is of critical importance in development of the material as a substrate for electronic and optoelectronic applications. First principles band structure approaches using a slab geometry are the initial tools of choice, and have been applied to the study of Pd and Pt overlayers on the (001) SrO- and TiO_2- terminated surfaces. Palladium and platinum are good candidates for epitaxial overlayer growth, due to the small lattice mismatch with the bulk titanate; Ochs et al. [170] and Asthagiri and Scholl [171] treated stoichiometric unreconstructed surfaces for Pd and Pd and Pt, respectively, concluding that for one ML or greater coverage, the TiO_2 | metal interface is more stable. Some predictions for initial growth modes of Pt overlayers were made, using 3×3 supercells (PP-DF, VASP) and small clusters Pt_n, $n = 1.5$ in pyramidal and flat arrangements. If history is a guide, this picture will be modified somewhat by the occurrence of defects such as oxygen vacancies and consequent surface reconstructions. Nevertheless, these calculations demonstrate the considerable degree to which theory is now able to complement experiment in deciphering surface growth modes and resulting surface structures.

As an example of the 'frontier' where hybrid theoretical modeling should be both valuable and interesting, we mention the recent development of mechanically compliant dielectric interface layers of the titanate as a component of an 'engineered interface' consisting of Si | SiO_x(amorphous) | $SrTiO_3$ | GaAs [172]. Here the superior electronic properties of GaAs needed for high speed switching are mated onto the more easily fabricated and controlled Si/silicon oxide substrate to make high performance devices. Note here the interplay of electronic, electrical transport, thermal conductivity, and mechanical properties characteristic of modern electronic materials design problems.

4.5. Oxide|oxide and oxide|metal interfaces: zirconia|Ni|NiO

ZrO_2 is a particularly interesting constituent of ceramic-metal interface structures due to its transparency, hardness, and high ionic conductivity-which can lead to interface degradation and failure, but which also may be exploited in high-temperature electrochemical applications [173]. Z-contrast scanning transmission electron microscopy (STEM) and electron energy loss spectroscopy (EELS) have been employed to analyze interfaces formed by reduction of NiO | ZrO_2(cubic) directionally solidified eutectics. A 17% reduction in the projected interface spacing, and comparison of the Ni $L_{2,3}$ EELS spectra with metallic Ni and Ni^{+2} in NiO led to the general conclusion that oxygen is removed from the interface, leaving metallic Ni in contact with Zr at the interface core. The prospect of in situ formation of nanostructured oxide–metal–oxide heterostructures suggests interesting possibilities for future device formation by 'growth' rather than by tedious vapor deposition [174].

Harel et al. reported electronic structure studies of ZrO_2 | Ni and ZrO_2 | NiO interfaces [175], and more recently Guo et al. carried out atomistic simulations and DF EC [GULP, DV] studies on Ni(111) | ZrO_2(100)(Cubic) and NiO(111) | Ni(111) | ZrO_2(100)-(Cubic) interfaces [176]. In order to accommodate the metallic Ni–Ni and Ni–ion interactions interatomic Morse potentials with parameters chosen to reproduce bulk metallic Ni and atom/ion radius sum rules were used, in addition to bulk-adjusted Buckingham parameters for Ni–O, Zr–O, and O–O interactions. Depth-profiling of atomic energies as a function of distance from the interfaces was used to determine the range of perturbations relative to the two bulk materials. The relaxed NiO (111)–Ni(111)–ZrO_2(100)(Cubic) periodic structure is shown in Fig. 6. The view is of the x–z plane, in a model which can be described as NiO($3_{[111]}$,$7_{[\bar{1}10]}$,$1_{[\bar{1}\bar{1}2]}$) Ni($9_{[111]}$) ZrO_2($4_{[100]}$,$8_{[010]}$,$2_{[001]}$) where the integer index represents the number of repeats of the interplanar distance and the subscripts denote the crystallographic directions within each crystal. Among the features immediately apparent in this image are twinning at the Ni | NiO interface essentially identical to that seen in high resolution STEM studies. The rigid zirconia structure is seen to be hardly perturbed, while the softer NiO and Ni have accommodated to interfacial strains and the mismatch between the three different crystal structures (Fig. 6).

The DF calculations produce Mulliken populations and volume–charge analyses which confirm the general picture of rapid healing of constituent materials across the interfaces. The Ni charge profile, passing from Ni^0 metal to Ni^{+2} in NiO in ca. three layers should of course be included in future variable-charge potentials for atomistic simulation, as discussed previously. A PDOS diagram for the multilayer periodic slab shows a systematic broadening of the Ni bands with increasing distance from the interface and increasing metallic character. The Ni band shifts are small, consistent with XPS observations of Harel et al., despite the calculated changes in ionicity—this confirms the general effects of pinning the Ni 3d band to a local Fermi level.

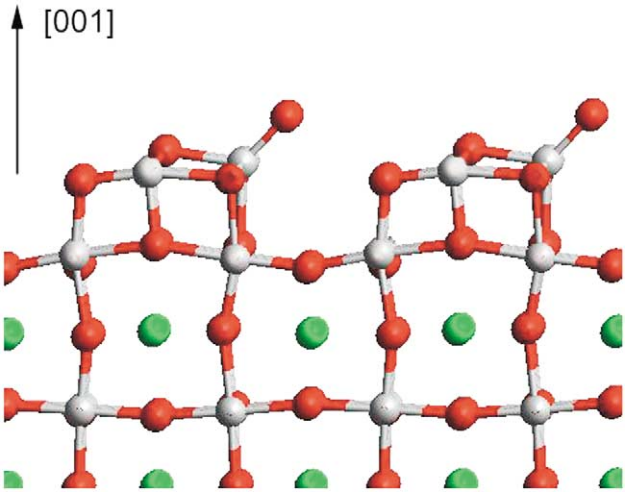

Fig. 5. TiO_2-rich (001)$SrTiO_3$ surface as determined from SXRD direct methods and DF-PP band structure atomic positions relaxation [162].

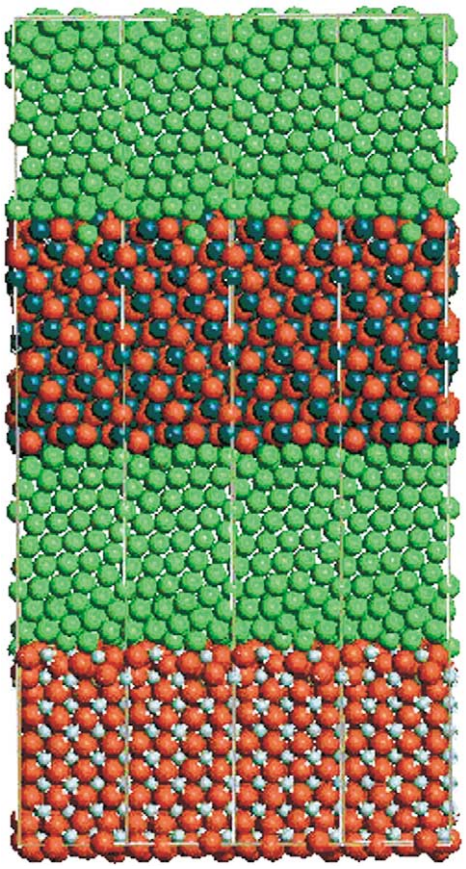

Fig. 6. X–Z plane arrangement of Ni–NiO–Ni–ZrO_2 periodic slab system. Frame lines denote supercell boundaries. From [176].

5. Conclusions

The ongoing evolution and development of hybrid quantum/classical methodologies is a critical part of the necessary effort to integrate a wide range of time- and length-scales needed to understand, predict, and control materials properties. We have shown how the component pieces such as first-principles HF, HF^+, and DF theory have been used initially as 'stand alone' tools, and more recently have begun to be operated in a systematic way to couple experiment, atomistic simulations, and statistical and thermodynamic approaches. The remarkable ability of simple parametrized interatomic potentials to reproduce observed properties of complex materials such as oxide surfaces and interfaces, and the enduring utility of the potential surfaces $E_i(X)$ as a guide to sampling and to structural surveys,

guarantees their continuing role as a bridging mechanism between different simulation and modeling regimes.

The status of several metal oxide interfaces, surfaces, and their interactions with adsorbant and impurity atoms and molecules has been briefly surveyed, in order to illustrate the interlinked analyses which are characteristic of advanced materials research. As we have moved from the era of idealized structures with a few degrees of freedom, toward a more realistic view where every atom can move, where structural and chemical defects often dominate reactivity and 'interesting' properties, we see very positive developments in integration of methodologies resulting in much improved predictive capability. The age of 'materials by design' may not have arrived yet, but it is measurably closer.

Acknowledgements

This research was supported by the US Department of Energy under Grant No. FG02 84ER45097. This work was also supported in part by the EMSI program of the National Science Foundation and the US Department of Energy Office of Science (CHE-9810378) at the Northwestern University Institute for Environmental Catalysis.

References

[1] A. Messiah, Quantum Mechanics, North-Holland, Amsterdam, 1962.
[2] G. Hertzberg, Molecular Spectra and Molecular Structure. Electronic Spectra and Electronic Structure of Polyatomic Molecules, vol. III, Van Rostrand Reinhold, New York, 1966.
[3] C. Kittel, Elementary Statistical Physics, Wiley, New York, 1958.
[4] J.H. Simmons, E.R. Fuller, Jr., A.L. Dragoo, E.J. Garboczi (Eds.), Computational Modeling of Materials and Processing, Amercian Ceramic Society, Westerville, OH, 1997.
[5] (a) J.C. Slater, The Self-Consistent Field for Molecules and Solids: Quantum Theory of Molecules and Solids, vol. IV, McGraw-Hill, New York, 1974;
(b) H.F. Schaefer, III (Ed.), Methods of Electronic Structure Theory, Plenum, New York, 1977;
(c) A. Szabo, N.S. Ostlund, Modern Quantum Chemistry—Introduction to Advanced Electronic Structure Theory, McGraw-Hill, New York, 1989.
[6] (a) R.G. Parr, W. Yang, Density Functional Theory of Atoms and Molecules, Oxford University Press, New York, 1989;
(b) D.E. Ellis (Ed.), Density Functional Theory of Molecules, Clusters, and Solids, Kluwer Academic Publishers, Dordrecht, 1995.
[7] (a) G.C. Schatz, M. ter Horst, T. Takayanagi, Computational methods for polyatomic bimolecular reactions, in: D.L. Thompson (Ed.), Modern Methods for Multidimensional Dynamics Computations in Chemistry, World Scientific, Singapore, 1998, p. 1;
(b) G.C. Schatz, Quantum effects in gas phase bimolecular collision processes: from state-to-state properties to microcanonical averages, in: W.L. Hase (Ed.), Comparisons of Classical and Quantum Dynamics. Advances in Classical Trajectory Methods, vol. 3, JAI Press, Greenwich, CT, 1998, p. 205;
(c) G.K. Schenter, B.C. Garrett, H. Gai, L.X. Dang, Comparison of classical and quantum statistical mechanical simulations of aqueous ionic clusters, in: W.L. Hase (Ed.), Advances in Classical Trajectory Methods: Comparisons of Classical and Quantum Dynamics, vol. 3, JAI Press, Greenwich, CT, 1998, p. 156.
[8] G.C. Schatz, Fitting potential energy surfaces, in: A. Lagana, A. Riganelli (Eds.), Reaction and Molecular Dynamics, Lecture Notes in Chemistry, vol. 14, Springer, Berlin, 2000, p. 15.
[9] G.K. Schenter, G. Mills, H. Jonsson, J. Chem. Phys. 101 (1994) 8964.
[10] G. Mills, H. Jonsson, G.K. Schenter, Surf. Sci. 324 (1995) 305.
[11] M.I. McCarthy, G.K. Schenter, C.A. Scamehorn, J.B. Nicholas, J. Phys. Chem. 100 (1996) 16989.
[12] W.M.C. Foulkes, L. Mitas, R.J. Needs, G. Rajagopal, Quantum Monte Carlo simulations of solids, Rev. Modern Phys. 73 (2001) 33.
[13] G. Rajagopal, R.J. Needs, W.M.C. Foulkes, W.M.C. Foulkes, S. Kenny, A. James, Phys. Rev. B51 (1995) 10591.
[14] (a) A. Rahman, Phys. Rev. 136 (1964) A405;
(b) M.L. Allinger, J.A. Hirsch, M.A. Miller, I.J. Tyminski, F.A. Van-Catledge, J. Am. Chem. Soc. 90 (1968) 1199;
(c) S. Nosé, J. Chem. Phys. 81 (1984) 511;
(d) S.J. Weiner, P.A. Kollman, D.A. Case, U.C. Singh, C. Ghio, G. Alagona, S. Profeta, Jr., P. Weiner, J. Am. Chem. Soc. 106 (1984) 765.
[15] G. Ciccotti, D. Frenkel, I.R. McDonald (Eds.), Simulation of Liquids and Solids, North-Holland, Amsterdam, 1987.
[16] M.P. Allen, D.J. Tildesley, Computer Simulation of Liquids, Clarendon Press, Oxford, 1987.
[17] F. Yonesawa, in: F. Yonesawa (Ed.), Molecular Dynamics Simulations, Springer, Berlin, 1992.
[18] (a) E.P.G. Areas, P.G. Pascotti, S. Schreier, K.C. Mundim, P.M. Bisch, J. Phys. Chem. 99 (1995) 14882;
(b) K.C. Mundim, C. Tsallis, Int. J. Quant. Chem. 58 (1996) 373.
[19] (a) N. Metropolis, A.W. Rosenbluth, A.H. Teller, E. Teller, J. Chem. Phys. 21 (1953) 1087;
(b) K. .Binder, D.E. Heermann, Monte Carlo Simulation in Statistical Physics, Springer, Berlin, 1988.
[20] L.J. LaBerge, J.C. Tully, Chem. Phys. 260 (2000) 183.
[21] See Refs [5,6] and J. Callaway, N.H. March, in: H. Ehrenreich, D. Turnbull, (eds.), Solid State Physics, Academic Press, New York, 1984;
(b) E.S. Kryachko, E. Ludena, Density Functional Theory of Many-Electron Systems, Kluwer Academic, Dordrecht, 1990.
[22] (a) P. Hohenberg, W. Kohn, Phys. Rev. 136 (1964) B864;
(b) W. Kohn, L.J. Sham, Phys. Rev. 140 (1965) A1133.
[23] (a) M. Levy, A. Nagy, Phys. Rev. Lett. 83 (1991) 4361;
(b) A. Nagy, Phys. Rep. 298 (1998) 1;
(c) A. Nagy, K.D. Sen, J. Chem. Phys. 115 (2001) 6300;
(d) A. Nagy, M. Levy, Phys. Rev. A6305 (2001) 2502;
(e) S.J.A. Gisbergen, C. Fonseca Guerra, E.J. Baerends, J. Comput. Chem. 21 (2000) 1511.
[24] (a) J. Callaway, Energy Band Theory, Academic Press, New York, 1964;
(b) W.A. Harrison, Solid State Theory, McGraw-Hill, New York, 1970.
[25] (a) D.E. Ellis, G.A. Benesh, E. Byrom, Phys. Rev. B 20 (1979) 1198;
(b) D.E. Ellis, J. Guo, H.P. Cheng, J. Phys. Chem. 92 (1988) 3024;
(c) D.E. Ellis, J. Guo, D.J. Lam, J. Am. Ceram. Soc. 73 (1990) 3231;
(d) D.E. Ellis, J. Guo, in: D.E. Ellis (Ed.), Electronic Density

Functional Theory of Molecules, Clusters, and Solids, Kluwer Academic Publishers, Dordrecht, 1995, p. 263.
[26] (a) W. Yang, Phys. Rev. Lett. 66 (1991) 1438;
(b) W. Yang, J. Mol. Struct. 255 (1992) 461;
(c) W. Yang, Z. Zhou, in: D.E. Ellis (Ed.), Density Functional Theory of Molecules, Clusters, and Solids, Kluwer Academic, Dordrecht, 1995, p. 177;
(d) Q. Zhao, W. Yang, J. Chem. Phys. 102 (1995) 9598.
[27] O. Warschkow, D.E. Ellis, J.M. Dyke, J. Comp. Phys. 143 (1998) 70.
[28] (a) R. Car, M. Parinello, Phys. Rev. Lett. 55 (1985) 2471;
(b) Q.M. Zhang, G. Chiarotti, A. Sellini, R. Car, M. Parinello, Phys. Rev. B42 (1990) 5071.
[29] L.J. Clarke, I. Štich, M.C. Payne, Comput. Phys. Commun. 72 (1992) 14.
[30] (a) I. Štich, D. Marx, M. Parinello, K. Terakura, Phys. Rev. Lett. 78 (1997) 3669;
(b) I. Štich, D. Marx, M. Parinello, K. Terakura, J. Chem. Phys. 107 (1997) 9482.
[31] G. Stapper, M. Bernasconi, N. Nicoloso, M. Parinello, Phys. Rev. B59 (1999) 797.
[32] C. Rovira, M. Parinello, Int. J. Quant. Chem. 80 (2000) 1172.
[33] I. Štich, M. Parinello, J.M. Holender, Phys. Rev. Lett. 76 (1996) 2077.
[34] E.S. Fois, J.N. Penman, P.A. Madden, J. Chem. Phys. 98 (1993) 6361.
[35] J.A. White, D.M. Bird, Phys. Rev. B50 (1994) 4954.
[36] M. Head-Gordon, J.C. Tully, J. Chem. Phys. 103 (1995) 10137.
[37] J.C. Burant, J.C. Tully, J. Chem. Phys. 112 (2000) 6097.
[38] J.C. Tully, M. Gomez, M. Head-Gordon, J. Vac. Sci. Technol. A11 (1993) 1914.
[39] C. Springer, M. Head-Gordon, J.C. Tully, Surf. Sci. 320 (1994) L57.
[40] (a) P.-O. Löwdin, Theor. Chim. Acta 89 (1994) 277;
(b) P.-O. Löwdin, Phys. Scripta 32 (1985) 261;
(c) B.N. Figgis, M.A. Hitchman, Ligand Field Theory and Its Applications, Wiley, New York, 1999;
(d) F.A. Cotton, Chemical Applications of Group Theory, 3rd ed, Wiley, New York, 1990, p. 287.
[41] E. Hernandez, M.J. Gillan, C.M. Goringe, Phys. Rev. B53 (1996) 7147.
[42] D.R. Bowler, M.J. Gillan, Comput. Phys. Commun. 120 (1999) 95.
[43] G.J. Ackland, D.M. Bird, P.D. Bristowe, M.W. Finnis, M.J. Gillan, V. Heine, P.A. Madden, M.C. Payne, A.P. Sutton, in: R.J. Allen, M.F. Guest, A.D. Simpson, D.S. Henty, D.A. Nicole (Eds.), High Performance Computing, Kluwer/Plenum Press, New York, 1999.
[44] (a) G. Kresse, J. Hafner, Phys. Rev. B47 (1993) 558;
(b) G. Kresse, J. Furthmüller, Phys. Rev. B54 (1996) 11169.
[45] C.K. Gan, P.D. Hayes, M.C. Payne, Phys. Rev. B63 (2001) 205109.
[46] T.L. Beck, Rev. Mod. Phys. 72 (2000) 1041.
[47] J.-L. Fattebert, J. Bernholc, Phys. Rev. B62 (2000) 1713.
[48] (a) W. Thiel, A.A. Voityuk, Theor. Chim. Acta 81 (1992) 391;
(b) W. Thiel, A.A. Voityuk, Theor. Chim. Acta 93 (1996) 315.
[49] J.C. Slater, G.F. Koster, Phys. Rev. 94 (1954) 1498.
[50] (a) D.W. Bullett, M.L. Cohen, Solid State Commun. 21 (1977) 157;
(b) D.W. Bullett, Solid State Phys. 35 (1980) 129.
[51] W.M.C. Foulkes, R. Haydock, Phys. Rev. B39 (1989) 12520.
[52] (a) T.N. Todorov, J. Phys.: Condens. Mat. 13 (2001) 10125;
(c) J. Purton, D.W. Bullett, P.M. Oliver, S.C. Parker, Surf. Sci. 336 (1995) 166.
[53] L. Feng, M.R. Press, S.N. Khanna, P. Jena, Phys. Rev. B39 (1989) 6914.
[54] H. Cruz, D. Luis, N.E. Capuj, L. Pavesi, J. Appl. Phys. 83 (1998) 7693.
[55] F.F. Abraham, Comput. Model. Eng. Sci. 1 (2000) 63.
[56] V. Rosato, M. Celino, J. Appl. Phys. 86 (1999) 6826.
[57] N. Bernstein, M.J. Aziz, E. Kaxiras, Phys. Rev. B58 (1998) 4579.
[58] (a) M.S. Daw, M.I. Baskes, Phys. Rev. Lett. 50 (1983) 1285;
(b) V.B. Deyirmenjian, V. Heine, M.C. Payne, V. Milman, R.M. Lynden-Bell, M.W. Finnis, Phys. Rev. B52 (1995) 15191;
(c) M.W. Finnis, J.E. Sinclair, Phil. Mag. A 50 (1984) 45;
(d) V. Heine, Solid State Phys. 35 (1980) 1;
(e) K.W. Jacobsen, J.K. Nørskov, M.J. Puska, Phys. Rev. B35 (1987) 7423;
(f) A.P. Sutton, J. Chen, Phil. Mag. Lett. 61 (1990) 139.
[59] (a) H.P. Cheng, D.E. Ellis, Phys. Rev. B39 (1989) 12469;
(b) H.P. Cheng, D.E. Ellis, J. Chem. Phys. 94 (1991) 3735;
(c) D.E. Ellis, H.P. Cheng, Electronic structure, cohesion and effective interatomic potentials in small transition metal particles, in: S. Sugano, Y. Nishina, S. Ohnishi (Eds.), Microclusters, Springer, New York, 1987, p. 63.
[60] V.B. Deyirmenjian, V. Heine, M.C. Payne, V. Milman, M.W. Finnis, Phil. Mag. Lett. 73 (1996) 39.
[61] (a) R.N. Barnett, R. Bass, J. Chem. Phys. 67 (1977) 4620;
(b) E.A. Colbourn, W.C. Mackrodt, Solid State Ionics 8 (1983) 221.
[62] G.V. Lewis, C.R.A. Catlow, J. Phys. C: Solid State Phys. 18 (1985) 1149.
[63] T.S. Bush, J.D. Gale, R.A. Catlow, P.D. Battle, J. Mater. Chem. 4 (1994) 831.
[64] J.D. Gale, J. Chem. Soc. Faraday Trans. 93 (1997) 629.
[65] D.H. Gay, A.L. Rohl, J. Chem. Soc. Faraday Trans. 91 (1995) 925.
[66] G.W. Watson, E.T. Kelsey, N.H. de Leeuw, D.J. Harris, S.C. Parker, J. Chem. Soc. Faraday Trans. 92 (1996) 433.
[67] M. Wilson, M. Exner, Y.-M. Huang, M.W. Finnis, Phys. Rev. B54 (1996) 15683.
[68] (a) N.C. Pyper, J. Chem. Phys. 114 (2001) 4390;
(b) N.A. Marks, M.W. Finnis, J.H. Harding, N.C. Pyper, J. Chem. Phys. 114 (2001) 4406.
[69] A.K. Rappé, W.A. Goddard, III, J. Phys. Chem. 95 (1991) 3358.
[70] F.H. Streitz, J.W. Mintmire, J. Adhes. Sci. Technol. 8 (1994) 853.
[71] S. Ogata, H. Iyetomi, K. Tsuruta, F. Shimojo, R.K. Kalia, A. Nakano, P. Vashishta, J. Appl. Phys. 86 (1999) 3036.
[72] (a) D. deFontaine, in: H. Ehrenreich, D. Turnbull (Eds.), Cluster Approach to Order–Disorder Transformations in Alloys. Solid State Phys. (1994) 33;
(c) J.M. Sanchez, F. Ducastelle, D. Gratias, Physica 128A (1984) 334;
(d) G. Ceder, P.D. Tepesch, A.F. Kohan, G.D. Garbulsky, C. Coley, H.T. Stokes, L.L. Boyer, M.J. Mehl, B.P. Burton, in: J.H. Simmons, E.R. Fuller, Jr., A.L. Dragoo, E.J. Garboczi (Eds.), Computational Modeling of Materials and Processing, American Ceramic Society, Westerville, OH, 1997, p. 115.
[73] M. Asta, G.B. Olson, private communication.
[74] D. Fuks, S. Dorfman, E.A. Kotomin, Y.F. Zhukovskii, A.M. Stoneham, Phys. Rev. Lett. 85 (2000) 4333.
[75] B.J. Jesson, P.A. Madden, J. Chem. Phys. 113 (2000) 5935.
[76] (a) B.R. Brooks, R.E. Bruccoleri, B.D. Olafson, D.J. States, S. Swaminathan, M. Karplus, J. Comp. Chem. 4 (1983) 187;
(b) A.D. Mackerell, Jr., B. Brooks, C.L. Brooks, III, L. Nilsson, B. Roux, Y. Won, M. Karplus, in: P.R. Schleyer, et al. (Eds.), The Encyclopedia of Computational Chemistry, vol. 1, Wiley, Chichester, 1998, p. 271;
(c) T.L. Windus, M.W. Schmidt, M.S. Gordon, in: R.J. Kalia, P. Vashishta (Eds.), Toward Teraflop Computing and New Grand Challenge Applications, Nova Science Publisher, New York, 1995, p. 189;

(d) M.S. Gordon, M.A. Freitag, P. Bandyopadhyay, V. Kairys, J.H. Jensen, W.J. Stevens, J. Phys. Chem. 105 (2001) 293;
(e) J. Gao, M.A. Thompson (Eds.), Combined Quantum Mechanical and Molecular Mechanical Methods ACS Symposium Series, vol. 712, ACS, Washington, DC, 1998;
(f) K.C. Mundim, D.E. Ellis, Brazil J. Phys. 29 (1999) 199;
(g) D.E. Ellis, K. Mundim, V.P. Dravid, J.W. Rylander, in: A. Pechenik, R.K. Kalia, P. Vashishta (Eds.), Computer Aided Design of High Temperature Materials, Oxford University Press, Oxford, 1999, p. 350.

[77] (a) W.K. Liu, S. Jun, Y.F. Zhang, Int. J. Num. Meth. Fluids 20 (1995) 1081;
(b) T. Belytschko, Y. Kronganz, D. Organ, M. Fleming, P. Krysl, Comp. Meth. Appl. Mech. Eng. 139 (1996) 3;
(c) M. Fleming, Y.A. Chu, B. Moran, T. Belytschko, Int. J. Num. Meth. Eng. 40 (1997) 1;
(d) W.K. Liu, S. Hao, T. Belytschko, S.F. Liu, C.T. Chang, Int. J. Num. Meth. Eng. 47 (2000) 1343;
(e) G.J. Wagner, W.K. Liu, Int. J. Num. Meth. Eng. 50 (2000) 507.

[78] International Conference on Multiscale Materials Modeling, organized by Z.X. Guo, M.R. Winstone, Queen Mary University, London, June 2002.

[79] (a) C. Satoko, Chem. Phys. Lett. 83 (1981) 111;
(b) A. Berces, T. Ziegler, Top. Curr. Chem. 182 (1996) 41;
(c) L.Y. Fan, L. Versluis, T. Ziegler, E.J. Baerends, W. Ravenek, Int. J. Quant. Chem. Suppl. 22 (1988) 173.

[80] (a) M.Z. Bazant, E. Kaxiras, Phys. Rev. Lett. 77 (1996) 4370;
(b) M.Z. Bazant, E. Kaxiras, in: E. Kaxiras, J. Joannopoulas, P. Vashishta, R. Kalia (Eds.), Materials Theory, Simulations, and Parallel Algorithms, MRS Proceedings, vol. 48, Pittsburgh. Mater. Res. Soc. (1996).;
(c) K.C. Mundim, L.A.C. Malbouisson, S. Dorfman, D. Fuks, J. Van Humbeeck, V. Liubich, J. Molec. Struct. (Theochem.) 539 (2001) 191.

[81] A.R. Gerson, T. Bredow, Phys. Chem. Chem. Phys. 1 (1999) 4889.

[82] M.D. Towler, N.M. Harrison, M.I. McCarthy, Phys. Rev. B52 (1995) 5375.

[83] N. Erdman, L.D. Marks, unpublished.

[84] A.M. Ferrari, G. Pacchioni, J. Phys. Chem. 99 (1995) 17010.

[85] E. Scorza, U. Birkenheuer, C. Pisani, J. Chem. Phys. 107 (1997) 9645.

[86] R. Orlando, R. Milini, G. Perego, R. Dovesi, J. Molec. Catal. 119 (1997) 253.

[87] L.N. Kantorovich, J.M. Holender, M.J. Gillan, Surf. Sci. 343 (1995) 221.

[88] L. Ojamäe, C. Pisani, J. Chem. Phys. 109 (1998) 10984.

[89] E. Giamello, M.C. Paganini, D.M. Murphy, A.M. Ferrari, G. Pacchioni, J. Phys. Chem. B 101 (1997) 971.

[90] D'Ercole, E. Giamello, C. Pisani, L. Ojamäe, J. Phys. Chem. B 103 (1999) 3872.

[91] E. Giamello, M.C. Paganini, D.M. Murphy, A.M. Ferrari, G. Pacchioni, J. Phys. Chem. B 101 (1997) 971.

[92] E.A. Colbourn, W.C. Mackrodt, Surf. Sci. 117 (1982) 571.

[93] E.A. Colbourn, Rev. Solid State Sci. 5 (1991) 91.

[94] H. Kobayashi, M. Yamaguchi, T. Ito, J. Phys. Chem. 94 (1990) 7206.

[95] R. Soave, A.M. Ferrari, G. Pacchioni, J. Phys. Chem. B 105 (2001) 9798.

[96] L.N. Kantorovich, M.J. Gillan, J.A. White, J. Chem. Soc. Faraday Trans. 92 (1996) 2075.

[97] A.M. Ferrari, S. Huber, H. Knözinger, K.M. Neyman, N. Rösch, J. Phys. Chem. B 102 (1998) 4548.

[98] S. Pugh, M.J. Gillan, Surf. Sci. 320 (1994) 331.

[99] P. Liu, T. Kendelewicz, E. Nelson, G.A. Parks, G.E. Brown Jr., SSRL Activity Report 1997, unpublished.

[100] (a) C.A. Scamehorn, A.C. Hess, M.I. McCarthy, J. Chem. Phys. 99 (1993) 2786;
(b) C.A. Scamehorn, N.M. Harrison, M.I. McCarthy, J. Chem. Phys. 101 (1994) 1547;
(c) J. Goniakowski, S. Buoette-Russo, C. Noguera, Surf. Sci. 284 (1993) 315;
(d) W. Langel, M. Parrinello, Phys. Rev. Lett. 73 (1994) 504;
(e) N.H. de Leeuw, G.W. Watson, S.C. Parker, J. Phys. Chem. 99 (1995) 17219;
(f) K. Refson, R.A. Wogelius, D.G. Fraser, M.C. Payne, M.H. Lee, V. Milman, Phys. Rev. B52 (1995) 10823.

[101] S. Abbet, U. Heiz, H. Häkkine, U. Landman, Phys. Rev. Lett. 86 (2001) 5950.

[102] J.N. O'Shea, J. Schnadt, S. Andersson, L. Patthey, S. Rost, A. Giertz, B. Brena, J.O. Forsell, A. Sandell, O. Bjorneholm, P.A. Brüwiler, N. Martensson, J. Chem. Phys. 113 (2000) 9233.

[103] A.M. Ferrari, L. Giordano, N. Rösch, U. Heiz, S. Abbet, A. Sanchez, G. Pacchioni, J. Phys. Chem. B 104 (2000) 10612.

[104] R. Yamauchi, I. Gunji, A. Endou, X. Yin, M. Kubo, A. Chatterjeee, A. Miyamoto, Appl. Surf. Sci. 130–132 (1998) 572.

[105] S. Abbet, U. Heiz, H. Häkkine, U. Landman, Phys. Rev. Lett. 86 (2001) 5950.

[106] R. Barnett, U. Landman, Phys. Rev. B48 (1993) 2081.

[107] S. Lee, S. Choic, S.-G. Oh, J. Korean Phys. Soc. 34 (1999) 93.

[108] G. Jordan, S.R. Higgins, C.M. Eggleston, Am. Mineralogist 84 (1999) 144.

[109] W. Wulfhekel, B. Heinrich, M. Klaua, T. Monchesky, F. Zavaliche, R. Urban, J. Kirschner, Appl. Phys. Lett. 78 (2001) 509.

[110] H.L. Meyerheim, R. Popsecu, J. Kirschner, N. Jedrecy, M. Sauvage-Simkin, B. Heinrich, R. Pinchaux, Phys. Rev. Lett. 87 (2001) 076102.

[111] W.H. Butler, X.-G. Zhang, T.C. Schultheiss, J.M. MacLaren, Phys. Rev. B63 (2001) 054416.

[112] D. Fuks, S. Dorfman, E.A. Kotomin, Y.F. Zhukovskii, A.M. Stoneham, Phys. Rev. Lett. 85 (2000) 4333.

[113] R. Baxter, P. Reinhardt, N. López, F. Illas, Surf. Sci. 445 (2000) 448.

[114] J. Guo, D.E. Ellis, D.J. Lam, Phys. Rev. B45 (1992) 13647.

[115] I. Manassidis, A. DeVita, M.J. Gillan, Surf. Sci. Lett. 285 (1993) L517.

[116] I. Manassidis, M.J. Gillan, J. Am. Ceram. Soc. 77 (1994) 335.

[117] I. Batyrev, A. Alavi, M.W. Finnis, Faraday Discuss. 114 (1999) 33 (This entire issue is devoted to metal oxide surfaces, with extensive theoretical and experimental analyses).

[118] (a) K.C. Hass, W.F. Schneider, A. Curioni, W. Andreoni, J. Phys. Chem. B 102 (2000) 5527;
(b) K.C. Hass, W.F. Schneider, A. Curioni, W. Andreoni, Science 282 (1998) 265.

[119] J.M. Wittbrodt, W.L. Hase, H.B. Schlegel, J. Phys. Chem. B 102 (1998) 6539.

[120] D.R. Jennison, A. Bogicevic, Faraday Discuss. 114 (1999) 45.

[121] R.M. Ferullo, M.M. Branda, G.R. Garda, N.J. Castellani, J. Molec. Catal. A-Chem. 167 (2001) 115.

[122] B.E. Eichinger, J. Stein, Surf. Sci. 492 (2001) 75.

[123] D.A. De Vito, F. Gilardoni, L. Kiwi-Minsker, P.Y. Morgantani, S. Porchet, A. Renken, J. Weber, J. Molec. Struct. Theochem. 469 (1999) 71.

[124] (a) J.R.B. Gomes, F. Illas, N.C. Hernandez, A. Marquez, J.F. Sanz, Phys. Rev. B65 (2002) 125414;
(b) J.R.B. Gomes, F. Illas, N.C. Hernandez, J.F. Sanz, A. Wander, N.M. Harrison, J. Chem. Phys. 116 (2002) 1684.

[125] I.G. Batirev, A. Alavi, M.W. Finnis, T. Deutsch, Phys. Rev. Lett. 82 (1999) 1510.

[126] R. Bennett, P. Stone, N. Price, M. Bowker, Phys. Rev. Lett. 82 (1999) 3831.

[127] H. Ohnishi, K.-C. Fukui, Y. Iwasawa, Bull. Chem. Soc. Jpn. 68 (1995) 2447.
[128] P.J.D. Lindan, N.M. Harrison, J. Holender, M.J. Gillan, M.C. Payne, Surf. Sci. 364 (1996) 431.
[129] P.J.D. Lindman ad, N.M. Harrison, Surf. Sci. Lett. 479 (2001) 375.
[130] P.J.D. Lindan, N.M. Harrison, J.A. White, M.J. Gillan, Phys. Rev. B55 (1997) 15919.
[131] M. Li, W. Hebenstreit, L. Gross, U. Diebold, M.A. Henderson, D.R. Jennison, P.A. Schultz, M.P. Sears, Surf. Sci. 437 (1999) 173.
[132] V. Swamy, J.D. Gale, Phys. Rev. B62 (2000) 5406.
[133] V. Swamy, J.D. Gale, L.S. Dubrovinsky, J. Phys. Chem. Solids 62 (2001) 887.
[134] V. Swamy, J. Muscat, J.D. Gale, N.M. Harrison, Surf. Sci. 504 (2002) 115.
[135] G. Charlton, P.B. Howes, C.L. Nicklin, P. Steadman, J.S.G. Taylor, C.A. Muryn, S.P. Harte, J. Mercer, R. McGrath, D. Norman, T.S. Turner, G. Thornton, Phys. Rev. Lett. 78 (1997) 495.
[136] B. Hird, R.A. Armstrong, Surf. Sci. 385 (1997) L1023.
[137] M. Ramamoorthy, D. Vanderbilt, R.D. King-Smith, Phys. Rev. B49 (1994) 16721.
[138] P. Reinhardt, B.A. Hess, Phys. Rev. B50 (1994) 12015.
[139] D. Vogtenhuber, R. Podloucky, A. Neckel, S.G. Stenneman, A.J. Freeman, Phys. Rev. B49 (1994) 2099.
[140] S.P. Bates, G. Kresse, M.J. Gillan, Surf. Sci. 385 (1997) 386.
[141] O. Gulseren, R. James, D.W. Bullett, Surf. Sci. 377-379 (1997) 150.
[142] A. Markovits, Surf. Sci. 497 (2002) 194.
[143] F. Rittner, R. Fink, B. Boddenberg, V. Staemmler, Phys. Rev. B57 (1998) 4160.
[144] T. Albaret, F. Finocchi, C. Noguera, A. De Vita, Phys. Rev. B65 (2002) 035402.
[145] P.J.D. Lindan, N.M. Harrison, J. Holender, M.J. Gillan, Chem. Phys. Lett. 261 (1996) 246.
[146] P.J.D. Lindan, N.M. Harrison, M.J. Gillan, Phys. Rev. Lett. 80 (1998) 762.
[147] R. Bennett, P. Stone, M. Bowker, Faraday Discuss. 114 (1999) 267.
[148] (a) M.M. Ameen, G.B. Raupp, J. Catal. 184 (1999) 112;
(b) M. Hossain, M.M. Ameen, G.B. Raupp, Adv. Environ. Res. 3 (1999) U1.
[149] P. Stone, R. Bennett, S. Poulston, M. Bowker, Surf. Sci. 433–5 (1999) 501.
[150] U. Diebold, M. Li, O. Dulub, E.L.D. Hebenstreit, W. Hebenstreit, Surf. Rev. Lett. 7 (2000) 613.
[151] P.L. Cao, D.E. Ellis, V.P. Dravid, J. Mat. Res. 14 (1999) 3684.
[152] N.N. Lathiotakis, A.N. Andriotis, M. Menon, J. Connolly, J. Chem. Phys. 104 (1996) 992.
[153] E. Heifets, R.I. Eglitis, E.A. Kotomin, J. Maier, G. Borstel, Surf. Sci. Article 12846 (2002) xxx.
[154] E. Heifets, R.I. Eglitis, E.A. Kotomin, J. Maier, G. Borstel, Phys. Rev. B64 (2001) 23417.
[155] C. Cheng, K. Kunc, M.H. Lee, Phys. Rev. B62 (2000) 10409.
[156] (a) A. Kazimirov, D.M. Goodner, M.J. Bedzyk, J. Bai, C.R. Hubbard, Surf. Sci. 492 (2001) L711;
(b) G. Koster, G. Rijnders, D.H.A. Blank, H. Rogalla, Physica C 339 (2000) 215;
(c) M.S.M. Gonzalez, M.H. Aguirre, E. Moran, M.A. Alario-Franco, V. Perez-Dieste, J. Avila, M.C. Asensio, Solid State Sci. 2 (2000) 519;
(d) B. Stauble Pumpin, B. Ilge, V.C. Matijasevic, P.M.L.O. Scholte, A.J. Steinfort, F. Tuinstra, Surf. Sci. 369 (1996) 313.
[157] T. Wolfram, R. Hurst, F.J. Morin, Phys. Rev. B15 (1977) 1151.
[158] M. Tsukada, C. Satoko, H. Adachi, J. Phys. Soc. Jpn. 48 (1980) 200.
[159] S. Kimura, J. Yamaguchi, M. Tsukada, S. Watanabe, Phys. Rev. B51 (1995) 11049.
[160] (a) J. Padilla, D. Vanderbilt, Surf. Sci. 418 (1998) 64;
(b) B. Meyer, J. Padilla, D. Vanderbilt, Faraday Discuss. 114 (1999) 395.
[161] (a) E.A. Kotomin, R.I. Eglitis, J. Maier, E. Heifets, Thin Solid Films 400 (2001) 76;
(b) E. Heifets, R.I. Eglitis, E.A. Kotomin, J. Maier, G. Borstel, Phys. Rev. B64 (2001) 235417.
[162] N. Erdman, K.R. Poeppelmeier, M. Asta, O. Warschkow, D.E. Ellis, L.D. Marks, Nature 419 (2002) 55.
[163] E. Heifets, E.A. Kotomin, J. Maier, Surf. Sci. 462 (2000) 462.
[164] (a) V. Ravikumar, D. Wolf, V.P. Dravid, Phys. Rev. Lett. 74 (1995) 960;
(b) M.C. Mackrodt, Phys. Chem. Mater. 15 (1988) 228.
[165] J. Torres, R. Viteri, A. Stashans, Abstract only:20th European Conference of Surface Science, Krakow, Poland, 2001.
[166] A. Stashans, F. Erozo, J. Ortiz, P. Valverde, Philos. Mag. B. 81 (1977) 2001.
[167] T. Yoshikawa, M. Bowker, Phys. Chem. Chem. Phys. 1 (1999) 913.
[168] R. Metzger, C. Werner, A. Spitzer, Thin Solid Films 365 (2000) 242.
[169] B.L. Kropman, D.H.A. Blank, H. Rogalla, Supramolecular Sci. 4 (1997) 59.
[170] T. Ochs, S. Kostlmeier, C. Elsasser, Integr. Ferroelectr. 32 (2001) 959.
[171] A. Asthagiri, D.S. Scholl, J. Chem. Phys. 116 (2002) 9914.
[172] A. Demkov, J. Ramdani, Motorola Inc., Unpublished presentations, 2002.
[173] (a) T. Wagner, R. Kirchheim, M. Rühle, Acta Metall. Mater. 43 (1995) 1053;
(b) A. Revcolevschi, G. Dhalenne, Nature 316 (1985) 335.
[174] E.C. Dickey, V.P. Dravid, P.D. Nellis, D.J. Wallis, S.J. Pennycook, A. Revcolevschi, Microsc. Microanal. 3 (1997) 443.
[175] S. Harel, J.-M. Mariot, C.F. Hague, Sur. Sci. 269/270 (1992) 1167.
[176] (a) C.-X. Guo, O. Warschkow, D.E. Ellis, V.P. Dravid, E.C. Dickey, J. Am. Ceram, Soc. 84 (2001) 2677;
(b) C.-X. Guo, D.E. Ellis, V.P. Dravid, L. Brewer, Mat. Res. Soc. Symp. 654 (2001) AA4.5.1.